THE UNIVERSITY OF ADELAIDE

ISOTOPIC AND GEOCHEMICAL CONSTRAINTS ON PROTEROZOIC CRUSTAL GROWTH FROM THE MT. PAINTER INLIER

by B.F. SCHAEFER

November, 1993

Supervisors: J D Foden, M Sandiford

ISOTOPIC AND GEOCHEMICAL CONSTRAINTS ON PROTEROZOIC CRUSTAL GROWTH FROM THE MT PAINTER INLIER.

By

Bruce F. Schaefer B.Sc.

This thesis is submitted as partial fulfillment for the
Honours Degree of Bachelor of Science

Department of Geology and Geophysics
University of Adelaide
November 1993

National Grid Reference (SH - 54) 6737, 6837 1:100 000

TABLE OF CONTENTS

LIST OF TABLES AND FIGURES

Plates:

Key to abbreviations used in text and diagrams.

Although abbreviations are defined where appropriate throughout the thesis, in the interests of completeness and easy referencing a summary of all abbreviations is presented below:

BEG	British Empire Granite
bt	biotite
cd	cordierite
CHUR	Chondritic Undifferentiated Reservoir
COLG	Collisional Granites
cor	corundum
FHQ	Freeling Heights Quartzite
fspar	feldspar
Ga	Giga-anna, = billions of years before present.
GRV	Gawler Range Volcanics
gt	garnet
HREE	Heavy Rare Earth Elements
KI	Kangaroo Island
kspar	Potassium feldspar
LBF	Lady Buxton Fault
LFB	Lachlan Fold Belt
LREE	Light Rare Earth Elements
MAQ	Mount Adams Quartzite
Ma	Mega-anna, = Millions of years before present.
micro	microcline
MNG	Mount Neill Granite
mu	muscovite
OIA	Ocean Island Arc
ORG	Ocean Ridge Granites
phlog	phlogopite
plag	plagioclase
qtz	quartz
RCM	Radium Creek Metamorphics
REE	Rare Earth Elements
T_{CHUR}	Model age from CHUR
T_{DM}	Model age from depleted mantle
tour	tourmaline
VAG	Volcanic Arc Granites
WPG	Within Plate Granites
YP	Yagdlin Phyllite

ABSTRACT

The Mt Painter Inlier comprises sequences of Palaeo- Mesoproterozoic metasediments, granitoids and granites. The igneous suites are geochemically similar to penecontemporaneous Australian I- and A-type granites, and contain elevated immobile element concentrations relative to Phanerozoic analogues. The metasedimentary sequences indicate shallow water, intracontinental depositional environments and isotope studies suggest short transport distance and local provenance. Nd depleted mantle model ages for the oldest granitoids and metasediments are clustered around 2.1-2.4 Ga, with the *younger* granitic units returning *older* model ages of 2.9-3.3 Ga. The 2.1-2.4 Ga event is correlated with events of similar age from other Australian terrains, and interpreted to represent a period of major continental crustal growth in Australia. The Archaean model ages for the younger granite suites are older than those of the neighbouring Gawler Craton, and may represent the juxtaposition of a hitherto undocumented Archaean terrain prior to ~1700 Ma. Proterozoic tectonic processes must therefore be responsible for the relative movement of stable cratonic nucleii on large scales in order to produce allocthonous juxtaposition. The Mt Painter Inlier therefore records an active tectonic evolution throughout the Proterozoic, incorporating continental crustal growth periods between 2.1-2.4 and at ~3 Ga. Tectonic activity continues to the present day, with both the Delamerian Orogeny and ongoing Tertiary thrusting processes being responsible for the current morphology of the inlier.

CHAPTER 1

1.1 Introduction

The evolution of continental lithosphere over geological time is the subject of much debate. Opinion is divided between uniformitarian and non- uniformitarian models for continental crustal growth mechanisms, and suggestions that crustal growth has been continuous over earth history (Gurnis and Davies, 1986), or episodic (Moorbath, 1977) must be considered against the possibilities that continental volume has remained constant (Armstrong, 1981; Armstrong, 1991) or decreased (Fyfe, 1978). The resolution of this problem is important as it has implications for the evolution of the thermal state of the earth (DePaolo *et al.*, 1991) and hence the driving mechanisms behind tectonic processes throughout earth history.

Approaches to resolving such problems are intimately related to the rates of growth and destruction of continental crust, as the mechanisms of growth and destruction of crust are a direct result of the controlling tectonic regime. Therefore, the question of continental crustal growth mechanisms offers insights into the debate on secular variations in the driving forces of orogenies over geological time (eg, Etheridge *et al.*, 1987). Radiogenic isotope tracers offer some insight into the source areas of sediments (McCulloch and Wasserburg, 1978), and the Sm-Nd system allows calculation of model ages which commonly reflect the age of mantle extraction for new crustal material (DePaolo and Wasserburg, 1976). This is limited in that Sm-Nd model ages do not reflect simple mantle extraction, but also mixing with some pre-existing material, and so constraining crustal growth on the basis of model ages may be misleading (DePaolo *et al.*, 1991). Using Sr isotopes to constrain the timing of major thermal events and trace element abundances to constrain the source regions of magmas, such data incorporated with the Sm-Nd system allows the problems of continental growth mechanisms throughout earth history to be elucidated (Jacobsen, 1988; McCulloch and Wasserburg, 1978).

1.2 Aims and Methods

This project is centred around the isotopic and geochemical investigation of the hitherto poorly explored Palaeo- Mesoproterozoic Mt Painter Inlier, and comparing data obtained with surrounding terrains in order to constrain periods and mechanisms of continental crustal growth.

The Mount Painter Inlier is a Proterozoic basement complex in the Northern Flinders Ranges of South Australia (figure 1). Exposures in the region are excellent, and

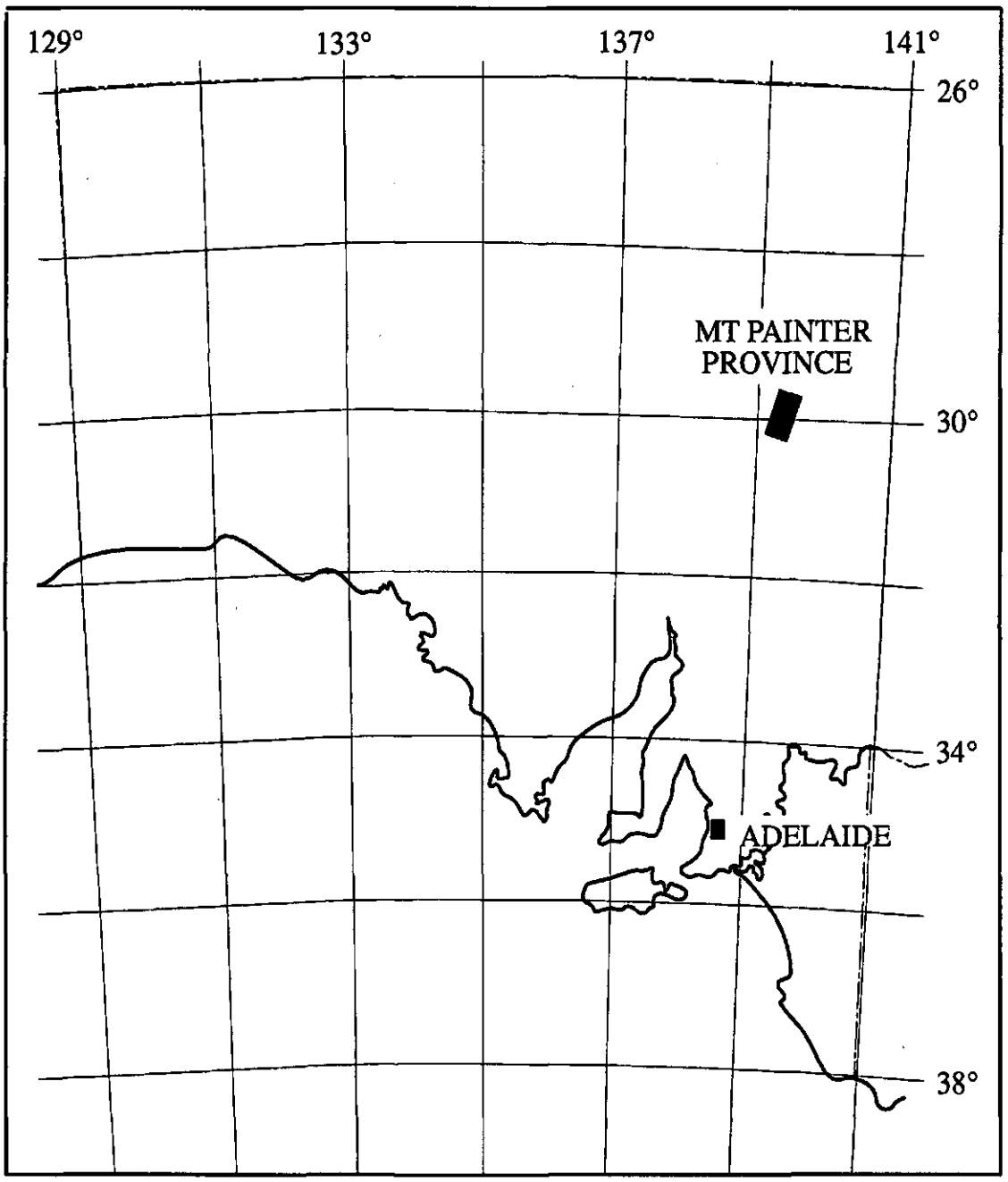

Figure 1: Location of the Mt Painter Inlier
in South Australia

the rock types (specifically igneous suites) offer an opportunity for isotopic and geochemical analysis. In order to achieve this, I have undertaken detailed mapping and analysis of both Proterozoic and Palaeozoic rocks within the inlier, and compared and contrasted the inherent isotopic and geochemical variations within them.

Mapping and analysis was done on a local scale within an area extending approximately 12 kms northeast of the Paralana Hot Springs (figure 2), followed by comparative analytical work within the inlier as a whole using the (scarce) data of other workers. Mapping was carried out over an 8 week period in conjunction with Teasdale (1993).

Where possible, this study incorporates data with surrounding basement terranes, specifically the Curnamona Cratonic Nucleus, the Broken Hill Block, the Mt Babbage Block and the Gawler Craton. Figure 3 shows the location of the Mt Painter Inlier in relation to these and other Precambrian tectonic provinces in Australia, many of which are referred to below (from Parker *et al.*, 1988).

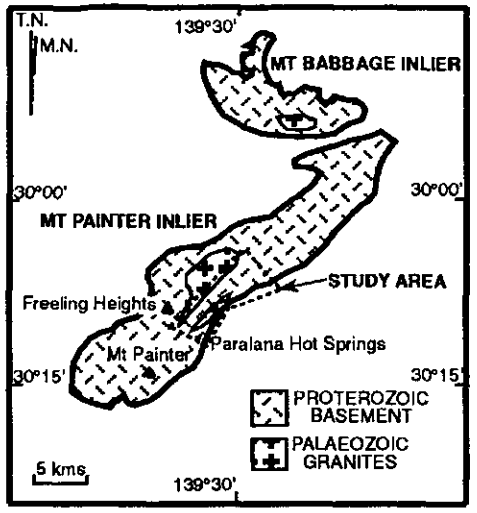

Figure 2:
Location of the study area in the Mt Painter Inlier.

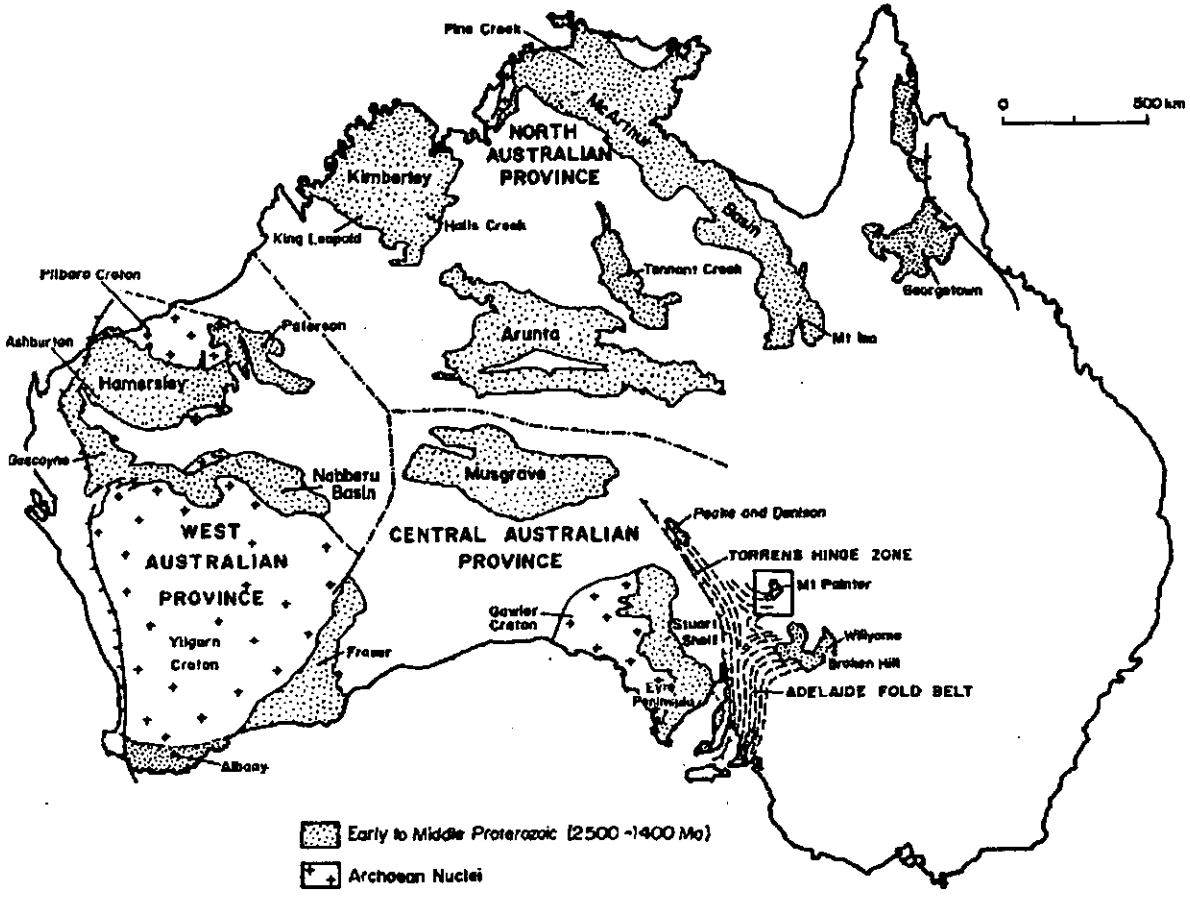

Figure 3:
Location of the Mt Painter Inlier with respect to other Australian Precambrian provinces.

CHAPTER 2 -REGIONAL GEOLOGY

In order to begin to evaluate mechanisms for crustal growth in a given area, it is first necessary to establish a sound geological framework from which to draw isotopic and geochemical data. This chapter aims to describe and evaluate the structure, occurrence and nature of the major lithologies encountered in the map area.

2.1 Previous Investigations

The Mt. Painter Inlier has been the subject of intense mineral exploration interest since the late 1800's, with particular emphasis on copper and uranium. The only regional mapping has been carried out by Coats and Blisset (1971), with localised mapping being conducted sporadically by mining companies and in various honours theses (eg Blight, 1975; Roberts, 1974). Recent work has focussed on the basement - Adelaidean unconformity (eg Mildren, 1992; Bingemer, *in prep.*) and its role in Delamerian metamorphism, however studies of the basement complex itself have been limited. Teale (1979; 1993 & *in press*) has published several papers refining stratigraphic nomenclature of various igneous suites within the basement, but to date a comprehensive revision has not been released. For this reason, the stratigraphy of the map area is based loosely on that of Coats and Blisset (1971) but also incorporating elements of that of Teale (1979 & *in press*).

2.2 Geology of the Paralana Hot Springs- Hidden Valley Area

The mapped area forms a strip extending northeast from Paralana Hot Springs to the northern end of Hidden Valley (figure 2), and comprises a complex series of Palaeoproterozoic para- and orthogneisses, Mesoproterozoic metasediments and felsic intrusives and assorted Phanerozoic granites and sediments. A brief summary of the lithologies observed is presented in figure 4 below.

2.2.1 Lithological Descriptions

As shown on figure 4, it is clear that the stratigraphy of the map area may be broadly divided into Palaeoproterozoic, Mesoproterozoic and Adelaidean/Delamerian sequences. The following discussion is conducted on this basis, beginning with the oldest units.

PALAEOPROTEROZOIC:

Paragneisses:

The paragneissic sequence is the oldest coherent unit encountered in the map area, and displays a complex structural relationship with the orthogneisses. These occur in the southern half of the map area and comprise a sequence of sheared and in places proto-mylonitised migmatites, quartzites and sillimanite bearing gneisses.

POST-PALAEOZOIC	Plain sediments.
ORDOVICIAN	British Empire Granite.
	unconformity
TERTIARY	Valley Sediments.
	unconformity
MESO-PROTEROZOIC	Mt Neill Granite.
	Freeling Heights Quartzite.
	Mt Adams Quartzite.
	Yagdlin Phyllite.
	unconformity
PALAEO-PROTEROZOIC	Orthogneisses.
	Paragneisses, inc. sill. gneiss

Figure 4: Simplified stratigraphic column for the map area. Lithology names are based on Coats and Blisset (1971) and Teale (1979, 1993 & *in prep.*). See also figure 5 and text.

A series of quartzofeldspathic migmatites comprise the basal unit of this sequence. They contain distinctive remobilised layering with occasional biotite selvedges. They are limited in distribution, outcropping only in the hinge of a SW trending anticline along Hot Springs Creek. The structural location is the basis for placing the migmatites at the base of the paragneissic sequence.

The migmatites may be traced into massive quartz rich gneisses, with the mineralogy varying in response to initial bulk composition of the sediments. These are interpreted to represent high grade massive light brown - beige quartzites and sandstones, however all sedimentary structures have been overprinted. Verification of a sedimentary / non-igneous origin of this unit is that despite the absence of sillimanite, they are almost identical to the sillimanite gneisses in hand specimen and appear to grade into these away from anticlinal cores. Both have 40-60% quartz, and contain varying amounts of gt ± kspar ± plag, with phlog-mu schist interbeds and lenses. This has the effect of making the sillimanite gneisses difficult to distinguish from the metasediments in hand specimen.

Orthogneisses:

The orthogneissic sequence displays a complex contact relationship with the paragneisses, and is found in a strip extending NE-SW from the bottom of Hidden Valley to west of the Hot Springs.

The most voluminous unit within this sequence is the black and white gneiss, a term used to describe a number of strongly foliated gneisses ranging from a black qtz-bt granite gneiss through granodiorites to a lighter coloured quartzofeldspathic granite gneiss (photo 4). Typically however, this unit comprises a dark quartzofeldspathic (~45% qtz, 30% plag and 20% bt) granodiorite gneiss with an S tectonite biotite fabric wrapping around K-feldspar and plagioclase (up to 10mm) phenocrysts.

The black and white granite gneiss is cross cut by an orange red augen gneiss with phyllosilicates containing the same pervasive fabric, but having large (up to 5cm) qtz/K-feldspar augen. The augen gneiss typically contains up to 40% qtz, <35% microcline, ~15% plagioclase and 5-10% bt, and it is suggested that this gneiss was originally a granite with large feldspar phenocrysts.

Both the black and white gneiss and the augen gneiss are intimately related with a later stage amphibolite gneiss that is characterised by a strong fabric defined by phyllosilicates and mafic minerals of smaller (<0.5cm) grain size. The amphibolite gneiss contains varying amounts (30-60%) of hornblende (possibly pargasite) with qtz (~30%) and microcline making up the remainder of the rock. Some samples of this unit contained large zircons and are anomalously rich in radioactive elements.

A brick red qtz-kspar granite gneiss associated with all of the units described above appears in a range of locations within the orthogneissic sequence, and its relationship with the other units is somewhat unclear, although it does contain the same fabric as the units described above (photo 5). A distinct geochemical signature showing high LREE identifies this granite as A-type, and whether it postdates the other members of the orthogneissic

	Coats and Blisset 1971	Teale 1979 *& in press.*	Hidden Valley Area
PALAEOZOIC	"YOUNGER GRANITE SUITE" Mudnawatana Granite	Gordon Springs Granodiorite Mudnawatana Tonalite British Empire Granite	British Empire Granite
ADELAIDEAN	Wywyana Formation	Wywyana formation	?Tertiary or Wywyana
MESOPROTEROZOIC	"OLDER GRANITE SUITE" Wattleowie Granite Terrapinna Granite Yerila Granite Mt Neill Granite Porphyry	Nooldoonooldoona Trondjhemite Wattleowie Granite Terrapinna Granite Mt Neill Granite Unit 3: Pepegoona Porph. Unit 2: Mt Adams Qtzite Unit 1: Yagdlin Phyllite	Other Granites to the N. Mt Neill Granite + Pepegoona Porph. Freeling Heights Quartzite Mt Adams Quartzite Yagdlin Phyllite
PALAEOPROTEROZOIC	RADIUM CREEK METAMORPHICS Freeling Heights Qtzite Brindana Schist Pepegoona Porphyry Mt Adams Quartzite Yagdlin Phyllite	Unit 6: Metagranite/volcs Unit 5:Metaquartzites Unit 4: Metasediments Unit 3: Layered Gneiss Unit 2: Augen Gneiss Unit 1: Migmatite	PARAGNEISSES ORTHOGNEISSES Leucogranite Gneiss A-type Gneisses Amphibolite Gneiss Black & White Gneiss Sillimanite Gneisses Metasediments/quartzites Migmatites

Table 1: Comparison of lithological names used for units in the Hidden Valley- Paralana area.

sequence described above is open to interpretation. The geochemistry of this unit is dealt with in chapter 3.

Cross cutting all of the above is a late stage white qtz-plag-kspar leucogranite gneiss. In only a few outcrops along Four Mile Creek does this lithology display sufficient mica to show a fabric parallel to that of the other gneisses within the sequence (photo 6). In thin section, the leucogneiss displayed rare symplectites (qtz-fspar). For the purpose of simplicity, this unit is usually considered as late stage orthogneissic suite, but it has been observed to cross cut the paragneisses, implying a syn-orogenic origin for the orthogneisses as a whole.

The dominant feature of all of the gneisses described above is the pervasive fabric, isoclinal folding and their upper amphibolite facies metamorphic grade. The complex relationships (both intrusive and structural) between the orthogneisses and the paragneisses suggest that both sequences are likely to be Palaeoproterozoic in age.

MESOPROTEROZOIC:

The Radium Creek Metamorphics (RCM) of Coats and Blisset (1971) originally included many of the lithologies described above, but the term is used here to describe the series of relatively undeformed metasediments found on the eastern side of the Lady Buxton Fault* , as well as in the north and extreme southwestern corner of the map area towards Freeling Heights. The sequence is intruded by the Mt. Neill Granite (described below), and must therefore predate its intrusion. This imposes a minimum Mesoproterozoic age on the Radium Creek Metamorphics.

The basal unit in the sequence is the Yagdlin Phyllite, a series of finely laminated brown-green phyllites metamorphosed to lower amphibolite grade. Phlogopite rich interbeds are commonly corundum bearing near the intrusive contact with the Mt Neill Granite. Mineralogy commonly includes phlog ± bt ± qtz ± fspar ± mu ± sill ± and ± cor ± gt, with the sequence becoming more feldspathic and massive near the top.

The Yagdlin Phyllite grades conformably into the Mt Adams Quartzite, a massive brown- grey- pinkish feldspathic quartzite that contains some pelitic interbeds. Sedimentary structures are common, particularly heavy mineral banding and cross bedding. A single occurrence of corundum within this unit was observed in a schistose pelitic interbed near the contact with the Mt Neill Granite.

* The Lady Buxton Fault is the north easterly extension of the Paralana Fault system beyond Paralana Hot Springs.

While both the Yagdlin Phyllite and Mt Adams Quartzite are restricted to the eastern side of the Lady Buxton Fault, the next Mesoproterozoic unit in the study area was observed only in the extreme southwestern and northern end of the map area. This unit was one member of the many mapped by Coats & Blisset (1971) as Freeling Heights Quartzite, but the name is defined here to describe the Mesoproterozoic quartzite rather than incorporating the Palaeoproterozoic paragneisses. The Freeling Heights Quartzite comprises a massive clean quartzite (~65% qtz, 30% mu) with distinctive heavy mineral laminations in the area around Freeling Heights. In the north of the map area this unit is more typically a series of qtz + mu schists that are distinguished from the sillimanite gneisses by virtue of their open style (as opposed to isoclinal) folding and apparent lower metamorphic grade. Due to the absence of contact relationships between this and the other Mesoproterozoic units, its location within the stratigraphy is somewhat tenuous, and is based on purely structural grounds.

Intruding the Mesoproterozoic sedimentary sequence is the Mt Neill Granite (MNG). This is a heterogeneous, massive, commonly red weathering, quartz undersaturated porphyritic granite to granite-syenite with a fine grained red groundmass and medium to large euhedral to ovoid K-feldspar phenocrysts (photo 1). Typical mineralogy in hand specimen is ~35% qtz and 45% microcline. Variations within the MNG include mafic melt fractions showing classic mixing textures with the more felsic melt components, light grey groundmass granite with large spherical plagioclase phenocrysts, late stage amphibolites and bt rich xenoliths. The unit as a whole was emplaced as a shallow level intrusive/extrusive complex, displaying a contact intrusive relationship with both the Yagdlin Phyllite and the Mt Adams Quartzite.

Elsewhere in the Mt Painter Inlier are a number of Mesoproterozoic igneous suites, including the rapakivi style Terrapinna Granite, the Yerila Granite (Coats & Blisset, 1971), the Nooldoonooldoona Trondjhemite and Wattleowie Granite. Geochemical comparisons with these units are made in 3.1 (See also Teale 1993 & *in press*).

ADELAIDEAN / DELAMERIAN:

Intrusive into the Freeling Heights Quartzite is a medium to coarse grained, light grey- white coloured granite (photo 2) with extensive associated pegmatism called the British Empire Granite (Teale 1979). In hand specimen it commonly contains qtz + mu + plag ± micro ± bt, with tourmaline occurring around the margins of some pegmatites. The British Empire Granite displays a classic intrusive contact with the Freeling Heights Quartzite, containing large xenoliths of Freeling Heights Quartzite and other country rock.

Plate 1

Photo 1: Contact of Mt Neill Granite with Mt Adams Quartzite. Note large (undeformed) feldspar phenocrysts and change in matrix colour moving away from the contact, suggesting a chilled margin. The pervasive fabric is interpreted to be igneous in origin due to the undeformed nature of the phenocrysts. The Mt Adams Quartzite is a homogeneous, medium grained grey quartzite.

Photo 2: Typical British Empire Granite. Note the light colour, medium- coarse grain size and undeformed nature.

Photo 3: Valley fill sequence. The matrix is fine- medium grained light green quartz and biotite bearing breccia. Xenoclasts in photo include grey- green phyllites, brown quartzites and a large granite clast.

Photo 4: Black and white gneiss. Distinctly foliated quartzofeldspathic granite-granodiorite gneiss. The fabric pictured is typical of the orthogneissic sequence.

Photo 5: A-type orthogneiss displaying pervasive fabric and feldspar phenocrysts. Of note is the typical brick red colour of A-type granites in the map area, ie, both the orthogneisses and the Mt Neill Granite.

Photo 6: Photomicrograph of the leucogranite gneiss displaying biotite fabric of the same origin as that observed in the rest of the orthogneissic sequence. This gneiss is quartz rich with varying proportions of feldspars.

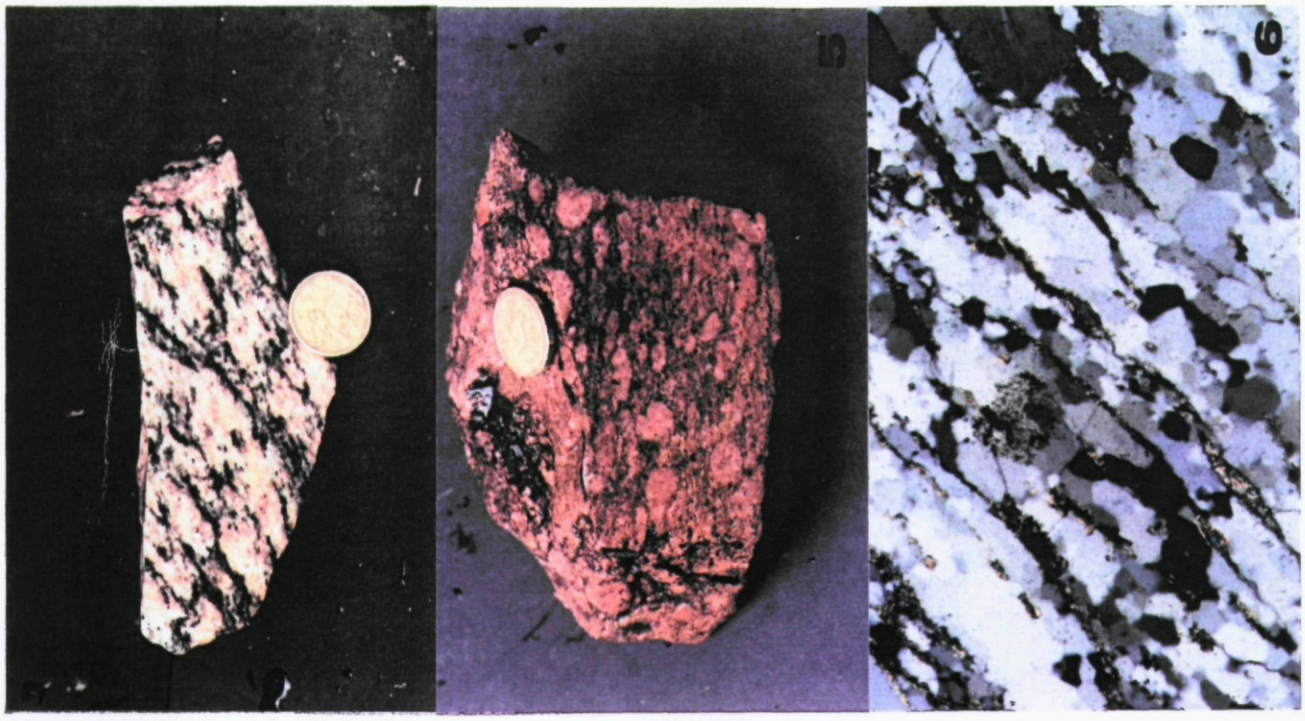
5
6

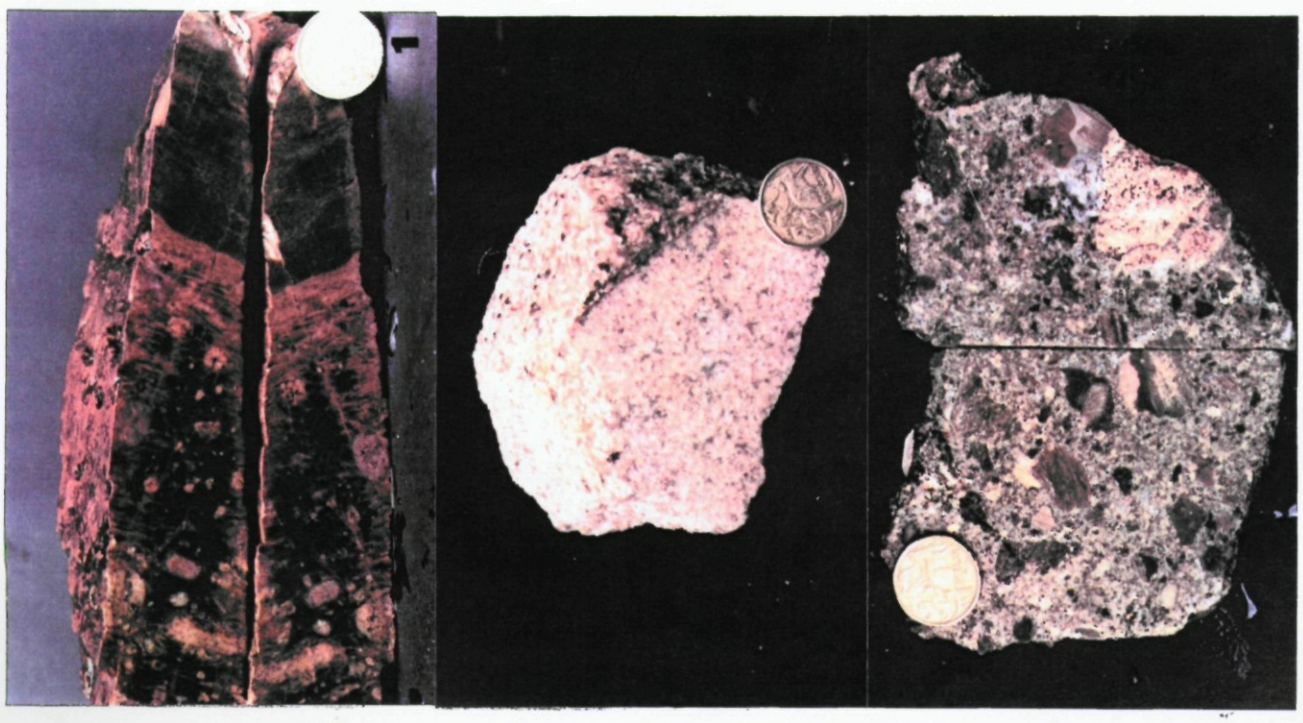
4

It is in the margins of these xenoliths that metasomatism occurs, typically in the growth of tourmaline.

The floor of Hidden Valley itself is a brecciated unit comprising a pale green groundmass of qtz ± mu ± bt ± tour (photo 3). The xenoclasts of material within this breccia are of great interest, ranging in size from several centimetres up to ~300m and comprise dominantly lithologies that are anomalous. Typically these are:

- Granulite facies gabbros and troctolite. One of the granulites is 2- pyroxene bearing, and quite unlike any other lithology in the map area.
- Mylonite, similar to that observed along the Lady Buxton Fault in the south of the map area.
- Feldspathic quartzites of unknown affinities (?Mt Adams Quartzite)
- Outcrops of both coherent and brecciated stratigraphy containing bedding and even preserved ripple marks. Previous workers (eg, Coats & Blisset 1971) have suggested this is Adelaidean Wywyana Formation.
- Calc-silicates of varying metamorphic grades.
- Calcite outcrops, the largest of which is 30 by 20m, &
- Pyrite clasts (<1cm).

This rock unit is extensively kaolinised at its margins. There are a number of differing theories as to the origin of this Valley Fill Sequence, several of which are outlined in 2.2.2 below.

MESOZOIC:

On the margins of the plains along the Eastern edge of the ranges there are a number of small exposures of a pale brown-white weathering sandstone, silicified in part. This unit contains Jurassic fauna to the north of Pepegoona Well.

TERTIARY:

Poorly sorted sands, clays and grits, associated with scarp foot conglomerates in a range of colours; typically brown-green to red and often kaolinised or ferruginised. These lithologies comprise the flat lying plains to the east, but near the edge of the ranges the beds may be observed to be vertical due to overthrusting of the basement complex.

2.2.2 Structure

The structure within the Paralana Hot Springs - Hidden Valley area displays a wide range of features and variations across lithologies, but may be summarised as shown in figure 6 below.

Within the Palaeoproterozoic paragneissic sequence, bedding (S_o) is occasionally suggested by transposed compositional variations within isoclinal folds (Teasdale 1993). The earliest recognisable deformation is that of the development of the sillimanite fabric (S_1), which may be observed to be subsequently isoclinally folded in some locations. The isoclinal folding (D_2) is typically of the order tens to hundreds of metres in scale, however within the black and white and amphibolite gneisses isoclinally folded K - feldspar veins may be observed.

D1	Development of sill. fabric, possibly parallel to bedding.
D2	Isoclinal folding event, F1. High T, Low P, M1.
D3	Open style folding, F2. Crenulation growth, F3.
D4	Tertiary uplift and probable thrusting, continued faulting and hydrothermal activity to the present day.

Figure 5: Summary of the major deformational events and their resultant structures in the Paralana Hot Springs - Hidden Valley area.

Open style folding within the Radium Creek Metamorphics (D_3, F_2) may be observed on a scale of kilometres, and is most pronounced within the Yagdlin Phyllite. This open style folding also folded the axes of the F_1 isoclinal folds. Associated with or formed shortly after was a pervasive crenulation within all major lithologies (F_3). Both the open style folding and the crenulation are truncated by the intrusion of the Mt Neill Granite, as observed by the presence of crenulations within rafts of corundum bearing schists along the intrusive contact. This therefore imposes a minimum age constraint on the timing of D_3.

Throughout the Phanerozoic there has been continued hydrothermal and faulting activity, with a thermal overprinting event suggested by isotope resetting (see 4.2 below). Although this does not constitute a discrete deformational event, this activity has been responsible for extensive brecciation and veining, and is probably related to Phanerozoic activity in the west of the inlier, around Mt Gee.

The last stage of deformation (D_4) is a process that is continuing today, that of Tertiary uplift and faulting; as observed in thrusting of the basement complex over the plains to the east and continued hydrothermal activity at the Paralana Hot Springs. It is this latest phase of uplift that is responsible for the present morphology of the region.

Of structural interest is the origin of Hidden Valley itself, and a summary of models proposed for this is presented below:

a) Diapirically emplaced Wywyana Formation: This model was first proposed by Coats & Blisset (1971), whereby the valley floor was composed of infaulted Callana Beds. While the Wywyana formation elsewhere in the inlier displays extensive mobilisation and diapirism into overlying units, movement of the Wywyana into the underlying basement is somewhat difficult to justify. The presence of biotite and muscovite in the matrix is inconsistent with the Adelaidean model due to the absence of these minerals in this lithology elsewhere in the inlier; and diapiric emplacement does not account for the gallimaufry of lithologies supported by the matrix.

b) Teale (*pers. comm.*) suggests that the valley floor is comprised of a volcanic breccia complex, such as that associated with a diatreme. This would explain the incorporation of anomalous granulites etc. in the breccia, these effectively being part of the Palaeoproterozoic basement sequence. This model however, has problems with respect to the proportion of biotite and muscovite in the matrix, the absence of volcanic layering and the presence of tourmaline crystals within the matrix, suggesting a sedimentary origin. The elongate shape of the valley is also difficult to reconcile with this model.

c) Another suggestion is that the valley floor is Tertiary sediment that has been brecciated by basement being overthrust on top of it. The overthrust block subsequently collapsed to the east, opening the valley as a window into the underlying (younger) sediments. The presence of biotite, muscovite and tourmaline in the matrix of the breccia are consistent with a sedimentary origin, and the gallimaufry of lithologies is a result of basement being dragged up along the thrust plane. Such thrusting over less dense material

(Tertiary sediments) adequately accounts for the regional bouguer gravity low over the Mt Painter Inlier. For a more detailed discussion on this model see Teasdale (1993).

The last model is entirely consistent with the ongoing tectonic processes observed in the Mt Painter Inlier today, and is favoured at the time of writing.

CHAPTER 3 -GEOCHEMISTRY

3.1 Geochemical Characteristics of the Granite Suites

Extensive XRF whole rock analysis was carried out on the three major suites of granites observed in order to:

a) establish lithological and magmatic affinities of the Palaeoproterozoic orthogneissic suite,

b) constrain the source regions and magmatic evolution of the Mt Neill and British Empire Granites and establish criteria for interregional correlation, and;

c) evaluate secular changes in magmas between the Proterozoic and the Phanerozoic.

3.1.1 Orthogneisses

XRF analysis (for information on analytical techniques, see Appendix E) on the orthogneissic sequence was conducted primarily for lithological discrimination; however some general observations may be made of the suite as a whole.

As a suite, the orthogneisses range in composition from granitic to granodioritic (figure 6a) and also encompass mafic and leucogranitic intrusive phases. They are generally silica saturated, however significant lithological variation does occur (see table 2b). A subdivision of the suite into I and A-type orthogneisses may be made on the basis of trace element abundances (figures 8 and 11). The orthogneisses are also characterised by high CaO values (reflected in figure 6b).

The orthogneisses are typically enriched in Sr and depleted in Rb in comparison with other granites from within the Mt Painter and Babbage Inliers (table 2a). They also display the characteristic elevated Zr levels of Proterozoic granites (Whalen *et al.*, 1987), and have a significantly lower K_2O/Na_2O ratio (<1, table 2a) than other igneous rocks in the inliers.

The Nb vs Y tectonic discrimination of Pearce *et al.* (1984) highlights the twofold subdivision of the suite, with samples plotting either in the volcanic arc / syn-collisional granite field (figure 10a) or the within plate field. The A-type granites are typically a brick red colour in hand specimen and display the pervasive fabric observed in the rest of the orthogneissic suite (photo 5). On figure 8 the A-types possess elevated LREE values. The relevance of incompatible element discrimination diagrams (such as figures 8 and 10) must be questioned, because in an area as extensively metamorphosed as the Mt Painter Inlier, there is some suggestion that extensive mobilisation of such elements (eg, Zr) has occurred

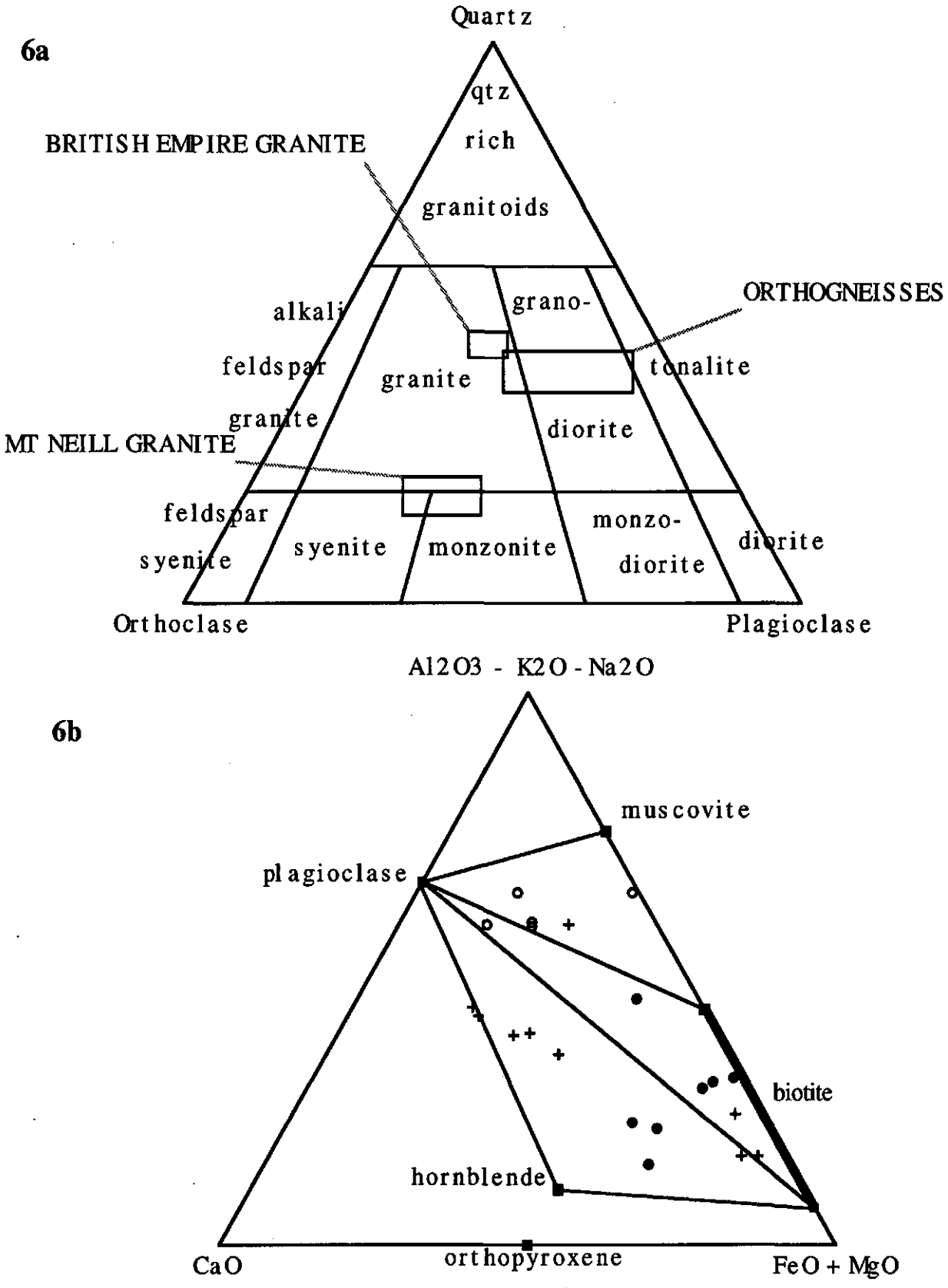

Figure 6: Ternary plots of the three igneous suites. **6a:** Classification of igneous suites by virtue of mineralogy. Note the syenitic - monzonitic nature of the Mt Neill Granite, and the spread across the granodiorite field by the orthogneissic sequence. **6b:** A-C-F discrimination diagram based on molar Al_2O_3 - K_2O - Na_2O, CaO and FeO + MgO. Open circles = British Empire Granite, closed circles = Mt Neill Granite; crosses = orthogneisses.

Table 2a: Comparison of average granite compositions within the Mt Painter and Babbage Inliers. (Data for Terrapinna, Wattleowie and Yerila Granites from Sheard *et al.* 1992.)

	BEG	MNG	GRANITE GNEISSES	TERRAPINNA GRANITE	YERILA GRANITE	WATTLEOWIE GRANITE
SiO2%	76.23	66.26	70.03	69.04	68.14	73.38
Al2O3%	13.61	14.40	14.67	14.06	13.06	12.88
Fe2O3%	0.83	5.71	3.40	4.16	5.94	2.11
MnO%	0.01	0.04	0.03	0.07	0.10	0.06
MgO%	0.18	2.01	1.20	0.89	1.01	0.33
CaO%	0.32	2.09	1.72	0.97	1.36	1.15
Na2O%	2.25	3.74	4.33	2.24	2.60	2.91
K2O%	5.76	4.04	3.41	5.65	4.81	5.34
TiO2%	0.08	0.89	0.51	0.49	0.60	0.26
P2O5%	0.05	0.15	0.10	0.14	0.15	0.11
SO3%	-0.01	0.01	0.01	-	-	-
LOI%	0.69	0.59	0.48	1.83	0.86	0.58
TOTAL %	99.98	99.91	99.88	99.54	98.63	99.11
Al Index	1.29	1.01	1.05	1.22	1.09	1.02
K2O/Na2O	2.56	1.08	0.79	2.52	1.85	1.84
Rb ppm	365.7	349.3	241.3	286	423	214
Ba	276.0	704.0	562.4	171	768	1013
Th	11.9	44.8	41.8	49	324	27
U	5.2	10.2	16.3	14	83	3
Nb	27.1	47.5	35.7	25	74	19
La	8.0	89.0	84.0	-	-	-
Ce	16.0	179.3	166.0	171	734	94
Pb	20.6	12.2	13.2	24	63	30
Sr	31.0	78.0	181.0	77	68	74
Nd	7.5	58.7	57.4	-	-	-
Zr	57.4	677.9	458.9	282	707	185
Sm	0.8	3.6	11.8	-	-	-
Y	29.7	145.3	93.3	61	171	41
Sc	5.6	21.3	13.3	-	-	-
Cr	16.5	17.2	13.9	-	-	-
V	6.7	90.4	43.7	-	-	-
Co	46.1	48.6	50.3	-	-	-
Ga	21.4	32.2	27.1	-	-	-
Cu	10.0	58.0	28.0	5	14	4
Zn	10.0	30.8	25.9	40	89	57
Ni	4.0	8.2	6.4	-	-	-
SAMPLES	5	9	9	16	14	9

BEG = British Empire Granite, MNG = Mt Neill granite.

- N.B. Average Sm values calculated from 1 sample for BEG, 3 samples for MNG and 3 samples for the orthogneisses.

Table 2b: Selected Whole Rock Analyses for the Orthogneissic sequence.

	I-TYPES						A-TYPES		
	leuco Paralana	*Plateau*	*leuco Paralana Ck*	*leuco Paralana Ck*	*augen gn. 4 mile Ck*	*leuco 4 mile Ck*	*Red gran Paralana Ck*	*Pink Paralana Ck*	*Red 4 mile Ck*
	BET-1	BET-2	92-2-2	92-2-8	HV-59	HV-84	92-2-3	HV-65	HV-87
SiO2%	72.44	70.03	72.51	73.06	77.96	73.54	68.52	70.68	74.95
Al2O3%	16.11	15.42	15.01	15.68	13.16	14.46	13.62	12.79	13.60
Fe2O3%	1.53	2.77	1.46	0.95	0.41	1.54	7.43	4.44	2.65
MnO%	0.02	0.05	0.02	0.02	0.00	0.03	0.03	0.02	0.01
MgO%	0.53	1.01	0.57	0.50	0.06	0.54	0.89	1.01	0.33
CaO%	3.20	2.43	2.14	2.64	0.19	1.79	0.36	0.43	0.15
Na2O%	5.07	3.34	4.29	5.51	6.93	3.68	6.37	1.83	7.35
K2O%	1.19	4.00	3.28	1.01	0.31	3.95	0.69	7.43	0.11
TiO2%	0.20	0.44	0.19	0.15	0.05	0.20	0.62	0.59	0.18
P2O5%	0.06	0.14	0.06	0.03	0.02	0.05	0.13	0.07	0.03
SO3%	0.00	0.00	0.01	0.02	-0.01	0.00	0.04	0.00	-0.01
LOI%	0.16	0.49	0.23	0.35	0.36	0.28	0.83	0.37	0.43
TOTAL	100.49	100.14	99.77	99.92	99.44	100.05	99.53	99.67	99.78
Al Index	1.04	1.08	1.04	1.05	1.09	1.06	1.15	1.08	1.09
K2O/Na2O	0.23	1.20	0.76	0.18	0.04	1.07	0.11	4.06	0.01
Ga/Al*10000	1.40	1.58	1.25	1.17	1.41	1.49	1.89	1.93	1.94
Zr+Nb+Ce+Y	136.50	298.00	135.40	188.40	93.00	177.90	1756.30	809.10	628.20
Rb	103.2	210.2	155.9	48.9	19.1	186.1	57.1	378.6	5.7
Ba	192.0	776.0	616.0	180.0	39.0	450.0	93.0	1080.0	19.0
Th	1.9	8.6	1.5	8.1	9.7	11.7	451.8	50.2	177.1
U	1.4	2.2	1.2	2.1	2.8	3.9	71.5	17.6	68.4
Nb	9.1	17.6	12.0	10.4	6.9	6.9	60.9	41.8	40.9
La	14.0	35.0	3.0	18.0	7.0	27.0	495.0	112.0	118.0
Ce	23.0	56.0	7.0	35.0	12.0	44.0	882.0	231.0	229.0
Pb	13.7	20.4	14.0	15.2	2.8	15.8	21.2	14.1	13.6
Sr	489.8	306.4	398.3	453.8	41.0	312.7	28.2	97.0	26.0
Nd	13.0	23.0	3.0	13.0	7.0	24.0	279.0	112.0	88.0
Zr	90.2	211.9	107.5	117.8	51.3	112.7	656.8	482.5	257.1
Sm	-	-	-	-	-	-	-	-	-
Y	14.2	12.5	8.9	25.2	22.8	14.3	156.6	53.8	101.2
Sc	5.7	6.2	5.6	7.1	0.9	3.7	9.8	14.7	1.6
Cr	11.0	16.0	20.0	24.0	3.0	-	-17.0	5.0	4.0
V	21.8	34.5	17.2	11.7	5.3	19.0	23.5	20.0	11.7
Co	48.2	35.6	30.0	70.5	83.1	37.4	31.8	61.8	45.4
Ga	22.6	24.3	18.8	18.4	18.5	21.6	25.8	24.7	26.4
Cu	9.0	7.0	3.0	3.0	11.0	5.0	106.0	34.0	8.0
Zn	34.0	51.0	20.0	12.0	8.0	33.0	16.0	16.0	9.0
Ni	8.0	13.0	4.0	2.0	4.0	11.0	3.0	8.0	7.0

Samples 92-2-2, 92-2-3 and 92-2-8 from Foden (*unpubl. data*)

Figure 7: Comparitive trace element geochemistry for the Mt Neill Granite (MNG), British Empire Granite (BEG), orthogneisses, Gawler Range Volcanics (GRV), and S-type granites from the Lachlan Fold belt (LFB) and Kangaroo Island (K.I.).

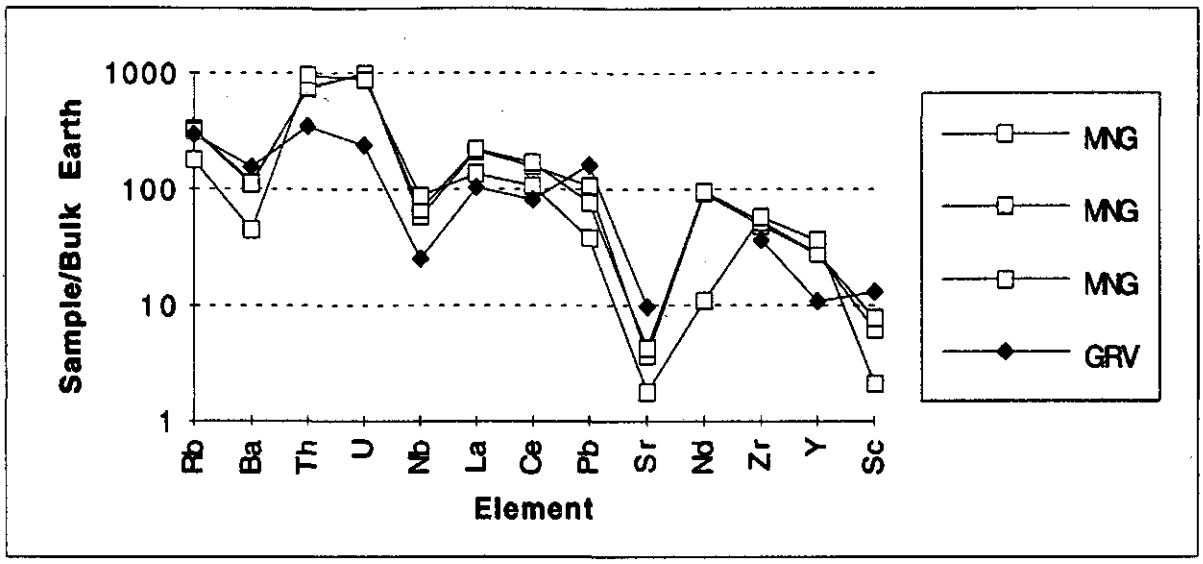

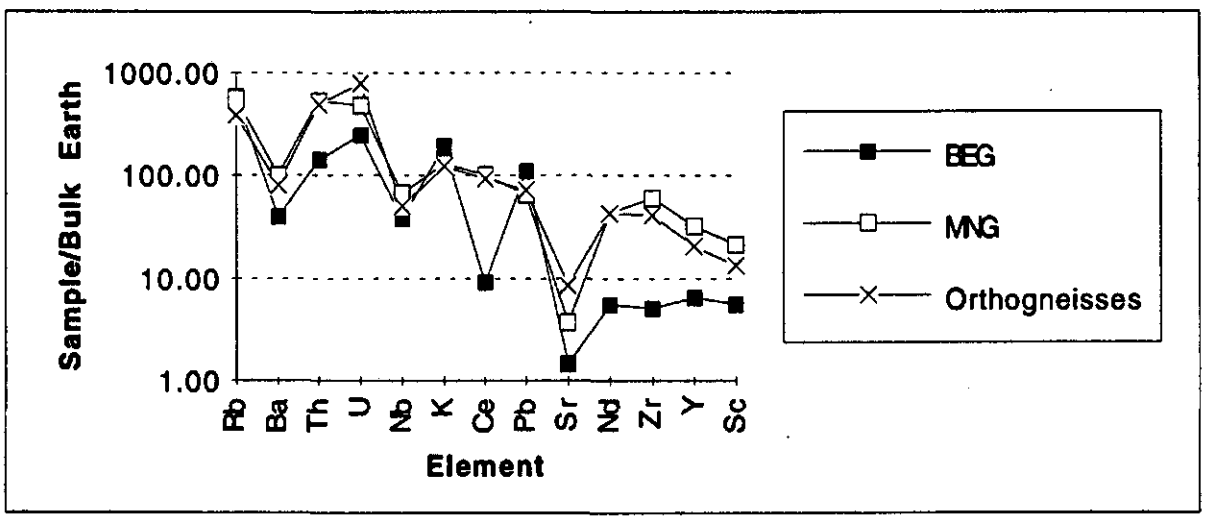

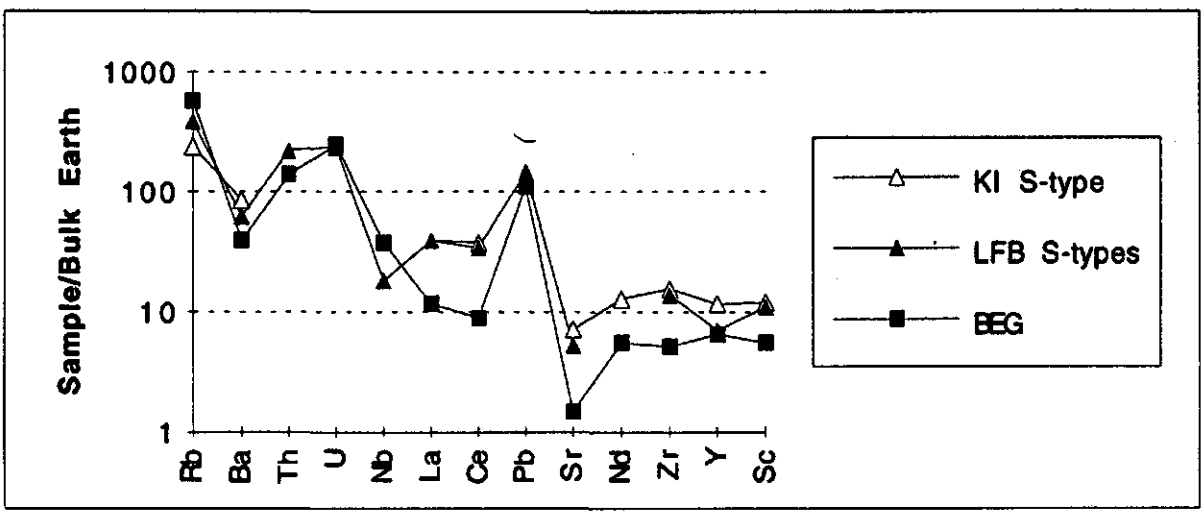

All samples normalised relative to values from Sun and McDonough 1989 Data for 92-2-1A and 1B from Foden (*unpubl. data)*, GRV from Creaser and White (1991), LFB from Chappell and White (1992) and KI from Turner *et al.* 1992.

(Benton, 1993). For the purposes of this study, it is suggested that such mobilisation is significant on the scale of individual minerals, but on a whole rock scale the abundances of incompatible elements reflect primary magmatic processes rather than metamorphic remobilisation.

The suite as a whole may be summarised as Palaeoproterozoic I and A-type granitoids, possibly forming from or as a result of a major crustal building episode at ~2.2 Ga (see Chapters 4 and 6).

3.1.2 Mt Neill Granite

The Mt Neill Granite (MNG) contains little free quartz in hand specimen, but what is present is a distinctive blue colour (photo 1). The range of SiO_2 values in the MNG results in a spread of compositions between granitic and syenitic (figure 6a), reflecting the heterogeneity of lithologies observed in the field. Classic mixing textures between mafic and felsic phases were observed, and the spread of SiO_2 values is a reflection of the heterogeneity within the source magma.

The MNG is typical of Proterozoic granites in that it contains elevated Zr, Ti and Y when compared to Phanerozoic analogues (Whalen *et al.* 1987). Coupled with high Th, La and Sc levels (table 2a and figure 7),a fractionated magma source is suggested by the high concentrations of immobile elements. Figure 11 (after Whalen *et al.* 1987) illustrates the enrichment of the MNG in Zr, Nb, Ce and Y relative to the BEG, and highlights the A-type nature of this unit. Figure 9 is a summary of the variations of incompatible element concentration, contrasting the MNG with the Palaeozoic BEG. Particularly distinctive are the plots involving Y, emphasising the depletion of incompatible elements in the BEG source.

Field relationships of the MNG display evidence of a very shallow level intrusion, particularly in the form of the mixing textures mentioned above, and also by the heterogeneity of the granite itself. Fabrics observed in cut samples near the intrusive contact with the Yagdlin Phyllite are interpreted as flow fabrics rather than tectonic due to the relatively unstrained nature of phenocrysts contained within (photo 1). Coupled with the mixing textures, a shallow intrusion depth is suggested, and proximity to the extrusive Pepegoona Porphyry to the north implies a comagmatic relationship. Unfortunately, insufficient geochemical data on the Pepegoona Porphyry has been published to allow unambiguous testing of this hypothesis.

Comparison of the MNG with the Gawler Range Volcanics (figure 7) results in almost identical trace element patterns, reflecting inherent similarities in the source regions of Mesoproterozoic A-type magmas. Of note is the depletion in Sr and Nb, and high values

Figure 8: Spidergram contrasting variations within the orthogneisses. The A-type orthoneisses contain elevated LREE values.

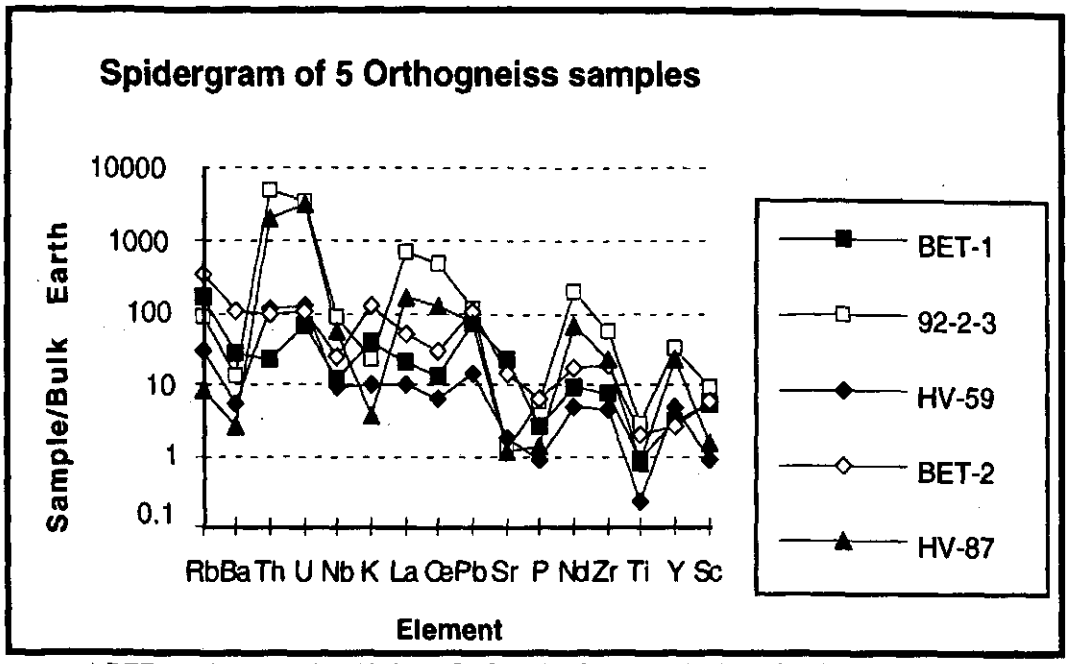

* BET-1 = Leucogneiss, 92-2-3 = Red gneiss from Hot Springs Creek, HV-59 = Augen gneiss from 4 mile Creek, BET-2 = Leucocratic phase within paragneisses and HV-87 = red gneiss from Hot Springs Creek.

Figure 9: Discrimination diagrams for the Mt Neill and British Empire Granites. Open squares with dots = British Empire Granite, filled diamonds = Mt Neill Granite.

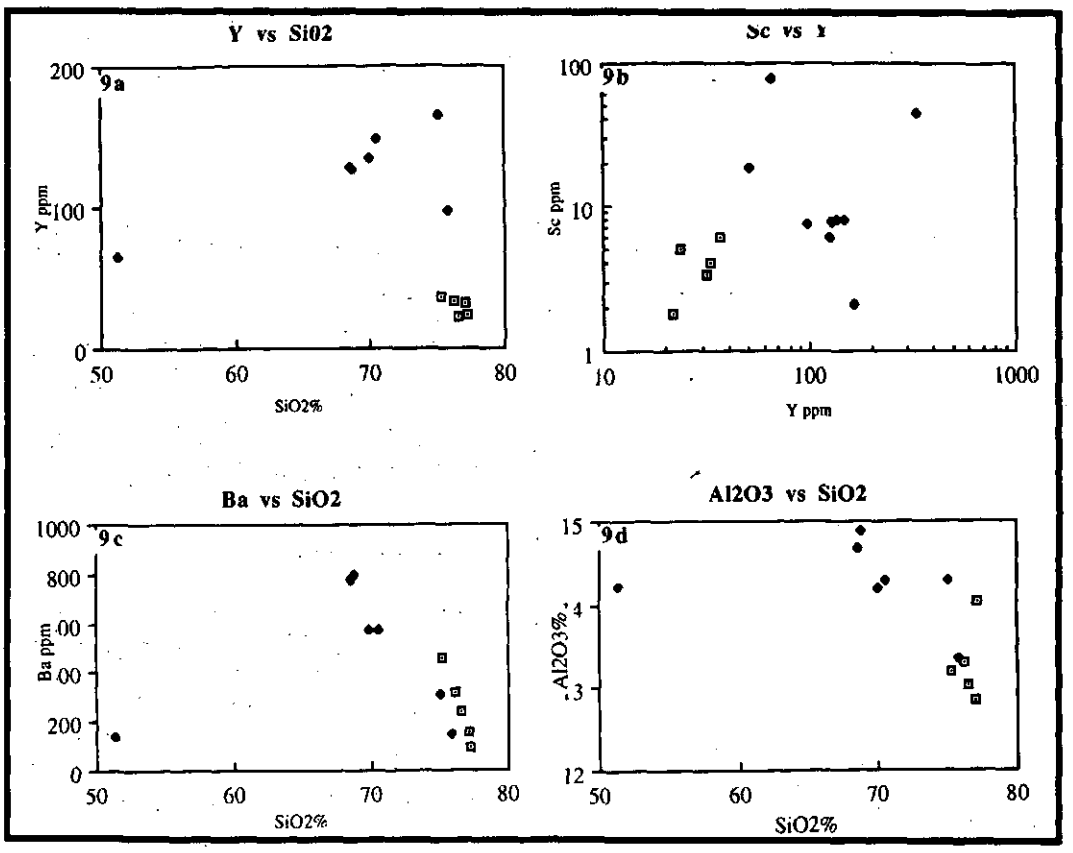

Table 3a: Summary of Whole Rock Analyses carried out on the Mt Neill Granite.

	Typical 92-2-1A	*Typical* 92-2-1B	*Nr camp* HV-12	*Valley Floor* HV-32	*Rnd Porphs.* HV-48	*S. of Valley* HV-57	*Amphibolite* HV-72
SiO2%	68.76	68.49	76.07	69.91	75.86	70.52	51.31
Al2O3%	14.88	14.67	14.29	14.20	13.35	14.28	14.21
Fe2O3%	4.30	5.06	0.87	3.79	0.82	3.77	13.86
MnO%	0.03	0.03	0.00	0.01	0.01	0.01	0.11
MgO%	0.28	0.37	0.18	1.27	1.31	0.32	6.30
CaO%	1.33	1.26	0.19	0.09	0.27	0.23	6.73
Na2O%	4.34	4.35	5.61	2.04	6.28	3.22	2.97
K2O%	4.88	4.56	3.26	6.71	1.00	5.93	1.29
TiO2%	0.41	0.44	0.40	0.49	0.37	0.51	2.26
P2O5%	0.07	0.07	0.05	0.05	0.06	0.09	0.43
SO3%	0.02	0.03	0.00	0.00	-0.01	0.00	0.00
LOI%	0.37	0.58	0.36	0.82	0.47	0.86	0.82
TOTAL	99.67	99.91	100.28	99.38	99.79	99.76	100.30
Al Index	1.00	1.02	1.09	1.32	1.12	1.18	0.77
K2O/Na2O	1.12	1.05	0.58	3.29	0.16	1.84	0.43
Ga/Al*10000	1.83	1.90	1.60	2.25	2.03	2.08	1.87
Zr+Nb+Ce+Y	993.20	1051.70	1054.20	1245.90	650.50	1332.60	441.10
Rb	206.2	200.4	112.0	311.9	88.2	429.8	147.7
Ba	801.0	772.0	309.0	573.0	148.0	574.0	140.0
Th	62.8	64.5	81.6	82.3	92.1	117.2	11.8
U	20.8	20.5	18.4	9.5	14.9	126.5	2.6
Nb	41.6	47.8	62.9	60.3	32.2	62.7	16.5
La	148.0	152.0	93.0	81.0	101.0	248.0	36.0
Ce	281.0	297.0	188.0	187.0	200.0	485.0	77.0
Pb	19.6	14.2	7.0	18.6	9.0	11.3	5.9
Sr	76.9	88.8	37.5	20.3	56.4	46.7	162.6
Nd	125.0	129.0	14.9	96.0	34.2	136.9	45.0
Zr	545.2	580.2	639.2	864.3	321.2	637.7	282.1
Sm	-	-	3.9	-	7.0	32.9	-
Y	125.4	126.7	164.1	134.3	97.1	147.2	65.5
Sc	6.1	7.7	2.1	8.1	7.6	8.0	48.3
Cr	3.0	1.0	2.0	2.0	8.0	2.0	79.0
V	3.2	3.2	2.3	2.6	22.5	7.2	310.1
Co	48.5	26.0	78.3	47.5	67.1	81.9	42.9
Ga	27.2	27.8	22.9	31.9	27.1	29.7	26.6
Cu	10.0	9.0	11.0	157.0	10.0	19.0	155.0
Zn	45.0	36.0	10.0	9.0	7.0	25.0	24.0
Ni	2.0	2.0	3.0	8.0	5.0	5.0	19.0

Samples 92-2-1A and 1B from Foden *(unpubl. data)*

Table 3b: Summary of Whole Rock Analyses from the British Empire Granite.

	948-92-BE1	948-92-BE2	948-92-BE3	948-92-BE4	HV-56
SiO2%	75.25	77.10	76.19	76.56	77.20
Al2O3%	13.19	12.84	13.30	13.04	14.03
Fe2O3%	1.18	0.49	0.57	0.19	0.47
MnO%	0.01	0.02	0.02	0.00	0.01
MgO%	0.23	0.14	0.14	0.08	0.12
CaO%	0.04	0.50	0.56	0.48	0.60
Na2O%	0.23	3.21	3.29	3.14	4.27
K2O%	8.31	4.52	4.66	5.59	3.20
TiO2%	0.12	0.05	0.06	0.03	0.04
P2O5%	0.05	0.10	0.09	0.07	0.04
SO3%	0.00	0.00	0.00	0.00	-0.01
LOI%	0.85	0.47	0.49	0.26	0.52
TOTAL	99.46	99.44	99.37	99.44	100.49
Al Index	1.40	1.16	1.16	1.08	1.21
K2O/Na2O	36.13	1.41	1.42	1.78	0.75
Ga/Al*10000	1.49	1.36	1.35	1.13	1.65
Zr+Nb+Ce+Y	159.00	110.40	105.20	67.90	101.30
Rb	499.0	293.8	327.6	250.3	232.4
Ba	460.0	152.0	317.0	241.0	92.0
Th	19.0	8.8	10.2	10.4	4.8
U	6.3	24.8	14.9	15.7	4.0
Nb	28.5	19.4	20.2	4.5	25.6
La	13.0	10.0	8.0	7.0	3.0
Ce	25.0	21.0	15.0	13.0	7.0
Pb	22.2	22.7	24.3	27.2	18.9
Sr	35.1	38.3	47.6	61.5	26.8
Nd	9.0	8.0	5.0	5.0	6.0
Zr	69.4	38.3	37.4	28.6	45.4
Sm	-	-	-	-	0.8
Y	38.1	31.7	32.6	21.8	23.3
Sc	6.0	3.4	4.0	1.8	5.1
Cr	29.0	31.0	29.0	29.0	4.0
V	8.2	4.4	5.1	3.8	5.2
Co	35.2	30.1	44.4	35.9	57.0
Ga	19.6	17.4	18.0	14.8	23.1
Cu	13.0	0.0	2.0	-	7.0
Zn	8.0	11.0	10.0	4.0	12.0
Ni	3.0	4.0	-	2.0	5.0

Samples 948-92-BE1 to 948-92-BE4 from Foden *(unpubl. data)*.

of Th and U. Roberts and Clemens (1993) suggest that such high K granites may be derived only from mafic to intermediate metamorphic rocks in the crust, and such a source appears consistent with the trace element chemistry observed (table 3a, figures 7 and 10).

Tectonic discrimination diagrams of Pearce *et al.* (1984) (figures 10b and 10c) suggest a within plate, anorogenic tectonic setting, consistent with the classification after Whalen *et al.* (1987) displayed in figure 11. The MNG is therefore interpreted to represent a typical Mesoproterozoic A-type shallow level intrusion sourced from previously depleted lower crustal material.

3.1.3 British Empire Granite

The grey-white British Empire Granite (BEG) is quite siliceous, as displayed by the abundance of free quartz in hand specimen (photo 2). The Al index and K_2O/Na_2O ratio shown on figure 8 indicate a strongly peraluminous nature which is specific to S-type magmas. SiO_2 values possess only a narrow range (75-78%, inc. data from Teale 1979), and particularly low MnO, MgO, CaO and TiO_2 values suggest a composition very close to that of a minimum melt (figure 6b).

The BEG displays distinctly different geochemical characteristics to the MNG, reflecting both its S-type nature and Palaeozoic age (table 3b). The Al_2O_3 vs SiO_2 discrimination diagram (figure 9b) reflects lower Al_2O_3 (compared to the MNG) values within the BEG, and figures 9 and 11 highlight variations in trace element composition between the two granite suites. The BEG contains lower concentrations of almost all trace elements measured and has lower Fe_2O_3 values suggesting derivation from a previously depleted source. Field relationships display the BEG intruding the Freeling Heights Quartzite (FHQ) and incorporation of FHQ into the melt may explain many of the geochemical characteristics observed. Figure 12b relates the BEG with the Radium Creek Metamorphics in terms of Al_2O_3 and SiO_2.

Figure 7 highlights the low concentrations of the BEG in trace elements by comparing it with the other igneous suite within the map area, and also compares the BEG with other S-type granites of similar ages. The BEG shows depletion in La and Ce, reflected in high Pb/Ce ratios relative to both I and other S-types, and also contains low levels of Nd, Zr, Ti and Y (figure 7).

The suggested tectonic setting for the BEG granite from Pearce *et al.* (1984) is syn-collisional bordering on orogenic (figure 10c); which is consistent with depletion of Nb & Y relative to the Proterozoic A and I-type granites. However, this tectonic setting is not consistent with field relationships.

Figure 10: Tectonic discrimination diagrams after Pearce *et al.* 1984

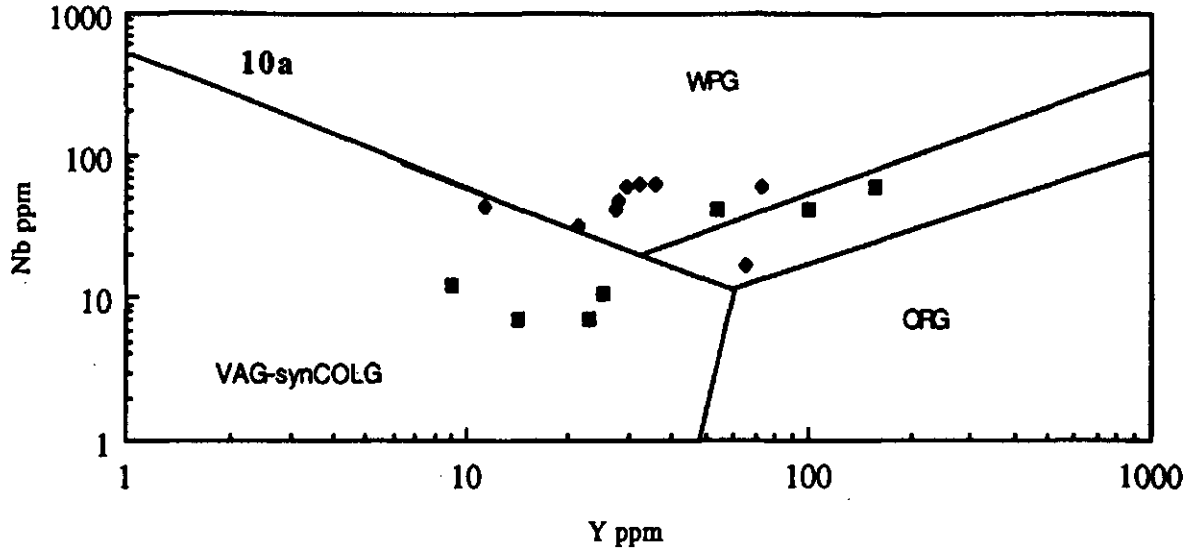

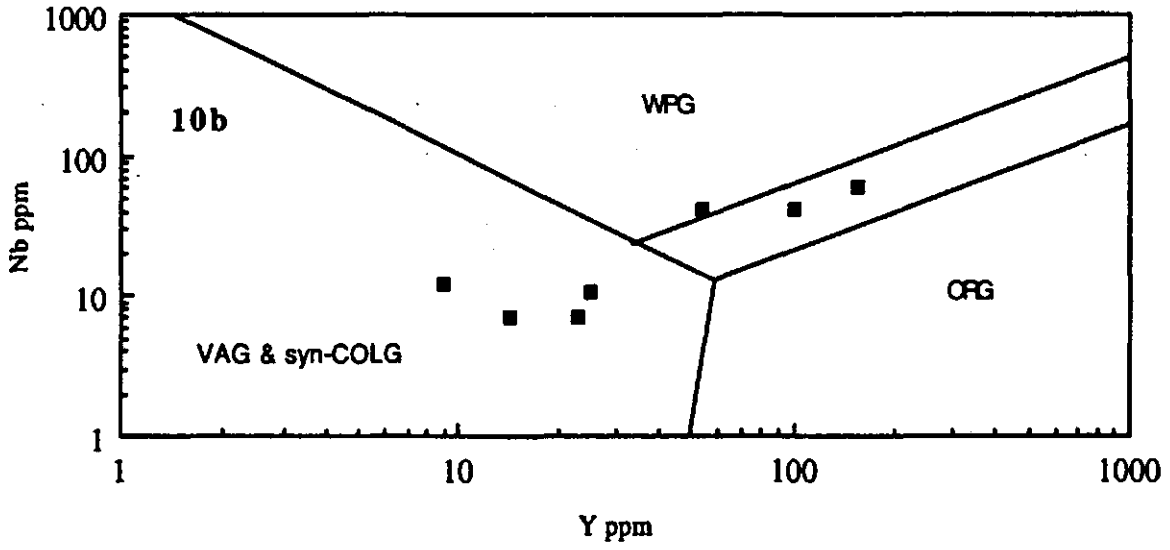

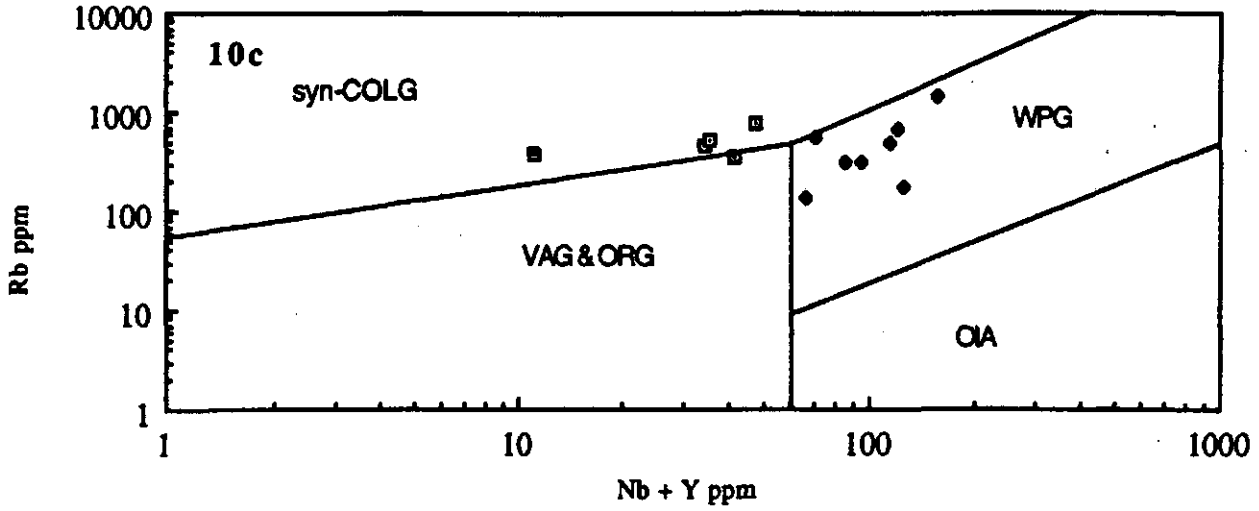

*Open squares with dots = BEG, black diamonds = MNG and filled squares with white dots = orthogneisses.

Figure 11: Discrimination diagrams of granite suites within the map area

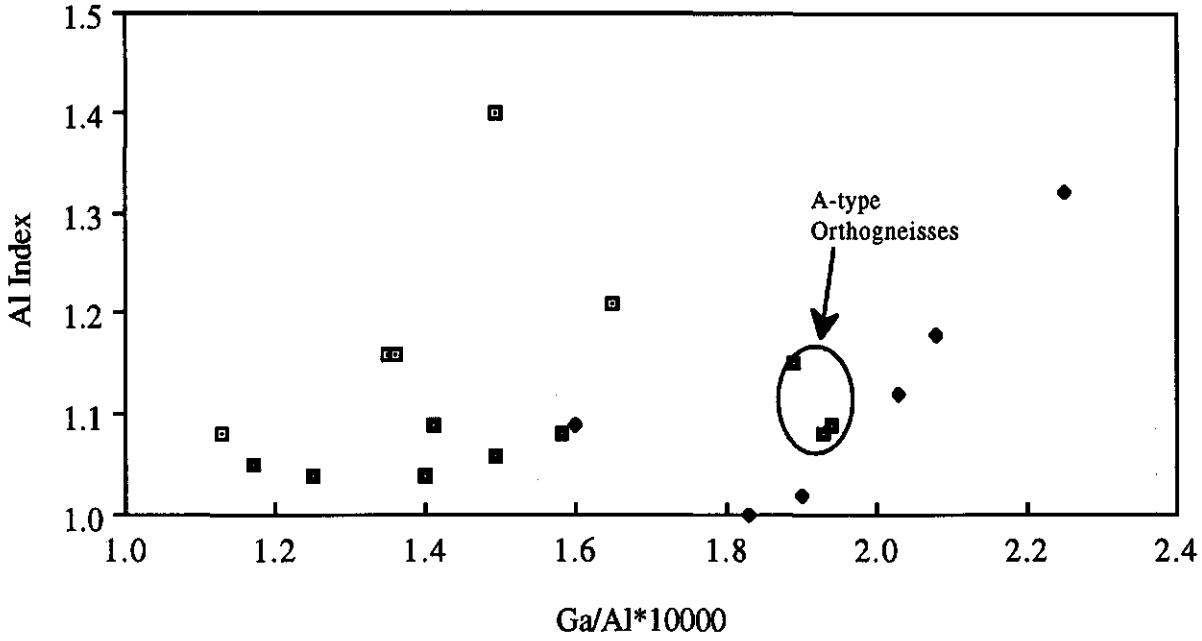

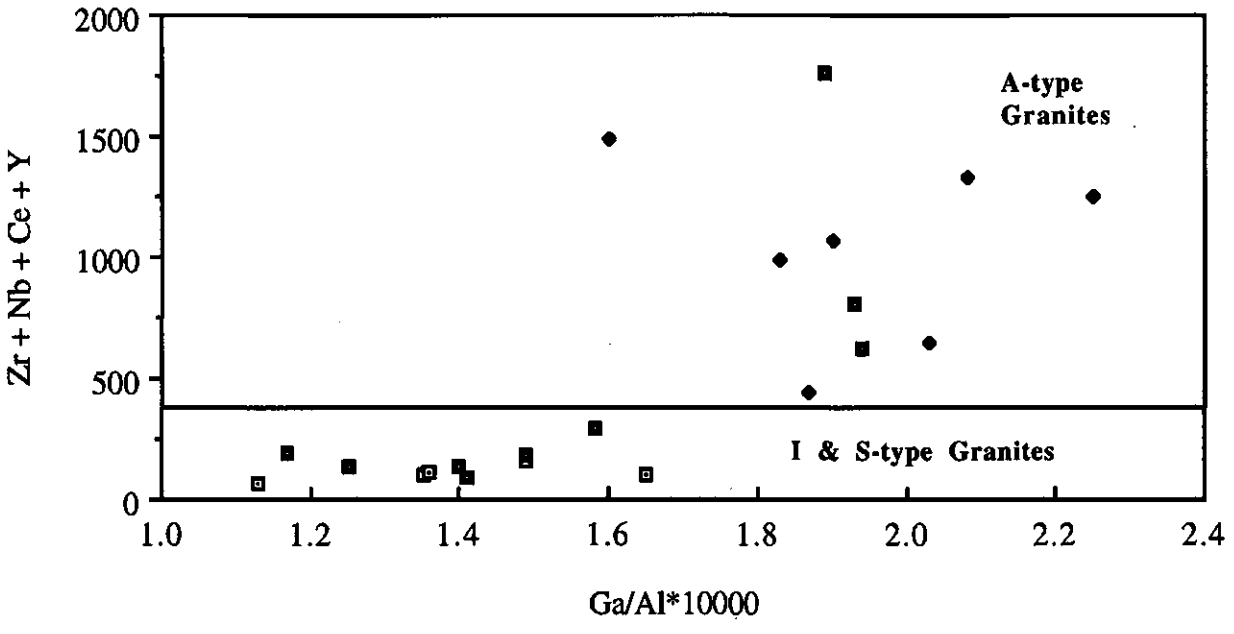

*Open squares with dots = BEG, black diamonds = MNG and filled squares with white dots = orthogneisses.

3.2 Geochemical Characteristics of the Metasedimentary Sequences

XRF whole rock analysis of both sequences of sedimentary rocks was carried out in order to establish any geochemical affinities of provenance areas and to delineate specific depositional environments. To this end, samples from the paragneissic sequence, Freeling Heights Quartzite (FHQ) and the Yagdlin Phyllite (YP) were analysed.

3.2.1 Paragneisses

The paragneissic sequence is dominated by massive, clean quartzites, and as such major element geochemistry reflects high silica levels and low FeO, MgO and CaO. By the same token, most trace elements have low values apart from Ti (which typically accumulates in a sedimentary environment) and Ba.

3.2.2 Radium Creek Metamorphics

The geochemistry of the Radium Creek Metamorphics (RCM) tends to reflect the sedimentary environment, with the finer grained, deeper water Yagdlin Phyllite (YP) containing high levels of silt and muds as opposed to the higher energy environment of the cleaner, more massive Freeling Heights Quartzite (FHQ).

The YP effectively acted as a sedimentary sump, concentrating most trace elements. The YP is significantly more aluminous than the FHQ, and contains higher levels of Th, Nb, Ga and Y (see figure 12). K_2O/Na_2O ratios for both the Paragneisses and the Radium Creek Metamorphics are extraordinarily high relative to both the igneous suites in the region, and the average Adelaide Geosyncline sediments (figure 13) (Turner *et al.*, 1992). Such elevated levels may reflect provenance from a region that already contains elevated K_2O/Na_2O ratios, such as a terrain that has had a minimum melt derived from it (ie, is enriched in biotite (Foden, *pers. comm.*), or it may be due to complex seawater buffering processes. Shales and phyllites generally contain higher ratios due to the large amount of biotite in them, but this does not account for elevated levels through sequences of different ages, such as the FHQ and the paragneisses (Glikson, 1983; Taylor and McLennan, 1983). Further comparison with Adelaidean and Lachlan Fold Belt sediments (Turner *et al.*, 1992) shows no consistent variations between the sedimentary sequences, suggesting that trace element geochemistry of sediments varies in response to their depositional environment, rather than reflecting secular variations in crustal composition.

The FHQ displays virtually no distinctive trace element variations; consistent with a high energy environment depositing a massive, clean quartzite.

Figure 12: Variation diagrams comparing metasedimentary sequences and British Empire Granite

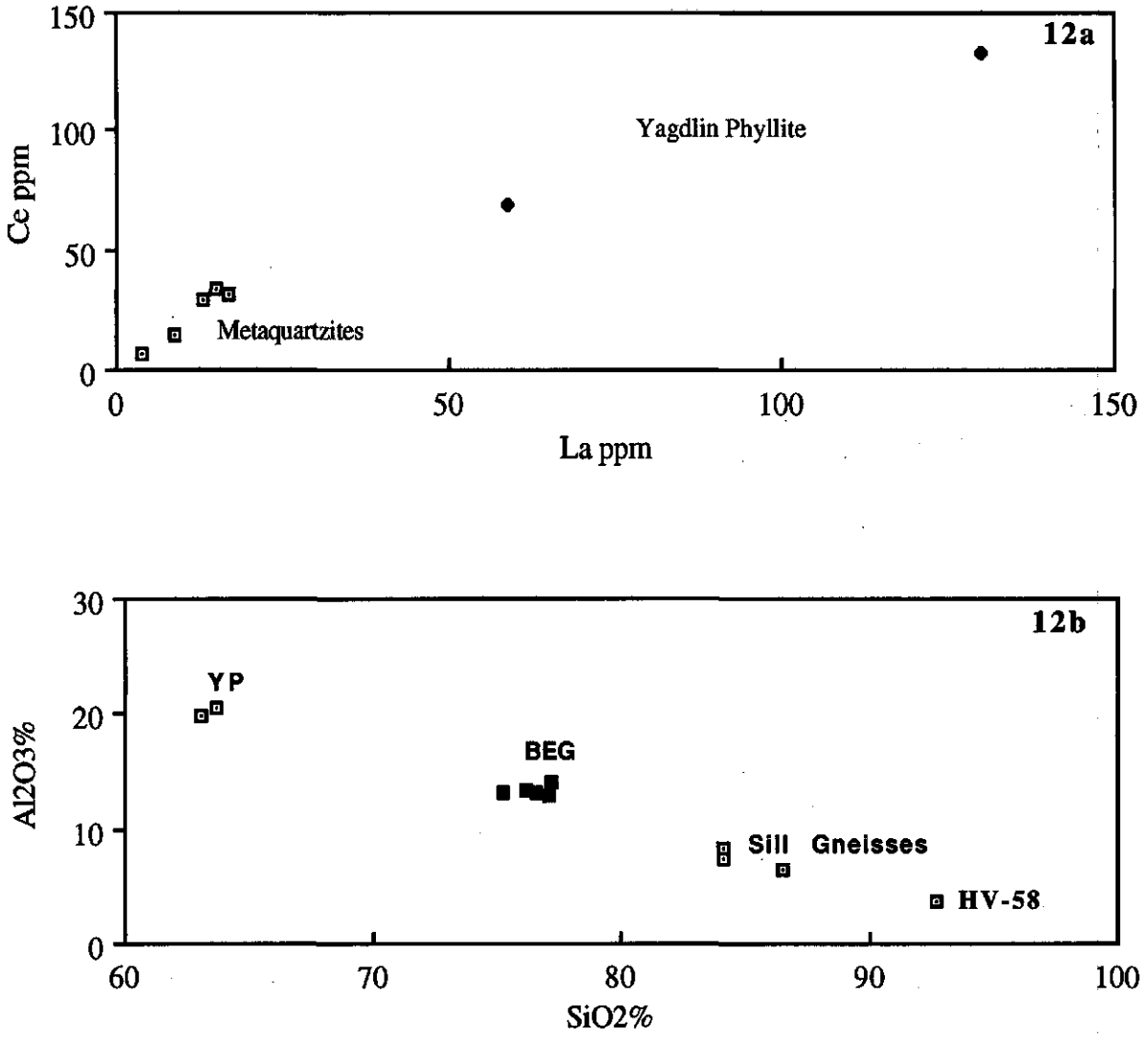

Figure 13: Al index vs K2O/Na2O for major lithologies. Note high values for the paragneisses.

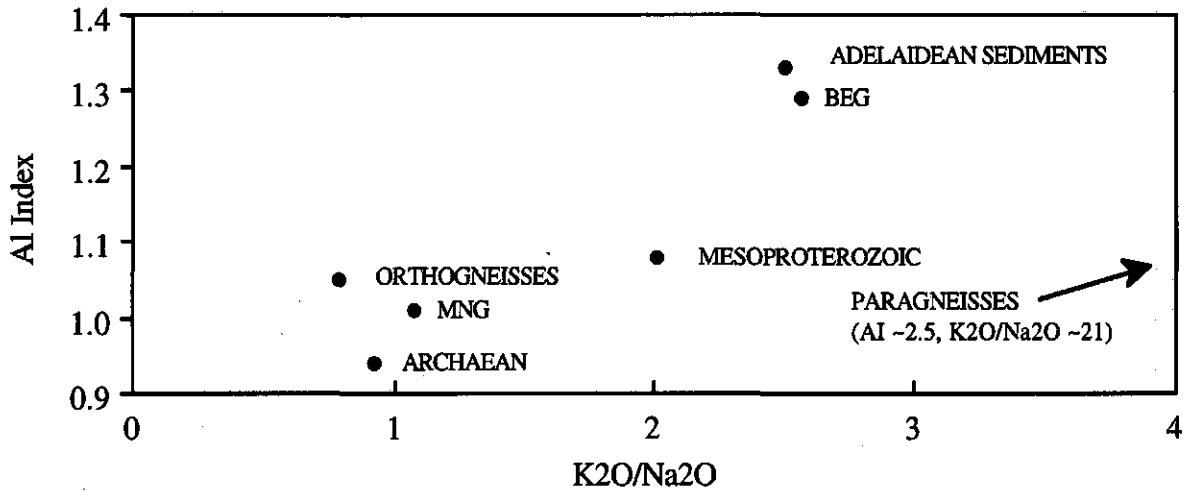

* BEG = British Empire Granite, MNG = Mt Neill Granite.

Data for Archaean, Mesoprot. and Adelaidean from Turner *et al.* 1992

The sedimentary sequences therefore contain geochemical signatures that are typical of variations observed in lithologies of sedimentary rocks of all ages, and apart from anomalous K_2O/Na_2O ratios, contain few distinctive geochemical markers.

CHAPTER 4: -ISOTOPE GEOLOGY

4.1 The Rb-Sr and Sm-Nd Isotope Systems

Isotope geology is based on the radioactive decay of a long lived isotope into a stable daughter product at constant rate that is unaffected by changes in pressure and temperature. As most elements have many isotopes, one or more of which may be are radioactive, the relative proportions of parent and daughter products effectively allow calculation of how long it has taken to accumulate a certain amount of a particular isotope by radioactive decay. This in effect acts as an atomic clock, and by measuring the relative abundances of isotopes of certain decay series, data pertaining to the age of mantle extraction, magma crystallisation and metamorphic overprinting of a rock may be obtained. Two commonly used radioactive decay systems in geochronology are the Rubidium - Strontium (Rb-Sr) and the Samarium - Neodymium (Sm-Nd) systems. A more detailed discussion on the principles behind isotope geology can be found in Appendix C.

The Rb-Sr isotope system is useful for age determination due to the wide range of Rb/Sr ratios present in many rock forming minerals and igneous rocks. However, this system is severely restricted in that both Rb and Sr are particularly mobile in the metamorphic environment (McCulloch & Wasserburg, 1978; Goldstein, 1988). This means the Rb-Sr system is readily reset during metamorphism, and only rarely may it be assumed that the system has remained closed since crystallisation. Therefore, in poly-deformed terranes where metamorphism and fluids have been active (such as the Mt Painter Inlier) remobilisation of Rb-Sr is anticipated.

Of particular importance in crustal evolution studies is the Sm-Nd system, which is particularly powerful because the parent/daughter pair are relatively immobile. This makes the system more robust and less susceptible to whole rock resetting during metamorphism than the Rb-Sr system. The calculation of model ages is quite useful as they suggest the age of extraction from the mantle of a magma. Sm/Nd model ages are preserved into the sedimentary cycle, not only preserving information on the provenance regions of sedimentary rocks, but also preserving the time of derivation of a certain part of the crust from the mantle. Therefore, Sm-Nd model ages of all types of rocks offer insights into the age of mantle extraction; however caution should be exercised when extrapolating such data to constrain periods of crustal growth (DePaolo, 1991; McCulloch and Wasserburg, 1978).

Data from the Sm-Nd system is commonly expressed in terms of epsilon notation (ε), which is the parts per 10000 difference in $^{143}Nd/^{144}Nd$ ratios between the sample and the Chondritic Uniform Reservoir, or CHUR. Therefore, a positive ε value (at a given

time) indicates a history of Light Rare Earth Element (LREE) depletion, and negative values indicate a history of LREE enrichment relative to a uniformly evolving mantle (DePaolo & Wasserburg, 1976). For more information on the calculation of model ages and epsilon values, see Appendix C.

In all isotopic systems described above, it is important that samples from within a single lithology have been in isotopic equilibrium with each other in order to obtain meaningful data.

4.2 Rb-Sr data and Interpretations

Sixteen whole rock samples from the Paralana Hot Springs - Hidden Valley area were analysed. Samples were selected from as wide a range of lithologies and locations as possible in order to constrain the ages of magmatic events and thermal overprinting.

Whole rock isochron ages were calculated, and the results are displayed in figure 18. The results suggest an age of 1700 Ma for the orthogneisses, 1069 Ma for the MNG and 384 Ma for the BEG. The BEG analysis includes whole rock data from Compston *et al.* (1966) on a pegmatite dyke in Arkaroola Creek, approximately 25km southwest of the map area but considered to be penecontemporaneous with the BEG. The isochron age for the BEG is similar to that of the MNG when data from a bitotite xenolith contained within the MNG is incorporated, resulting in a whole rock age of 405 Ma. The XRF analysis of the xenolith is very close to that of a biotite mineral separate, and therefore this lower age is interpreted to reflect a thermal resetting event above the closure temperature of biotite.

The resetting age of 405 Ma for the MNG, and the 384 Ma for the BEG are within error to an age of ~400 Ma from 9 samples obtained by Webb (1976) using the K-Ar technique, which has an even lower closure temperature than Rb-Sr. Sheard *et al.* (1992) also note that a number of the lower intercepts on U-Pb concordia from zircons in the granite suites give ages of 300 Ma or younger, representing Pb loss events during the Phanerozoic.

Of interest is the 1700 Ma age for the orthogneissic suite. Since this suite displays a pervasive fabric and amphibolite facies metamorphism, it is fair to assume that this age reflects a Palaeoproterozoic orogenic overprinting event. This age therefore places a minimum age constraint on the deposition of the paragneissic sequence, as the paragneisses contain the same fabrics and styles of deformation observed in the orthogneisses that developed during this event. The orthogneisses possess the lowest initial ratios in the map area, and a possible explanation for the preservation of such an old metamorphic Rb-Sr age in an area where extensive mobilisation has occurred may be that metamorphic fluid flow has been concentrated or channelled preferentially through specific lithologies.

Figure 14: Rb-Sr Whole rock isochrons

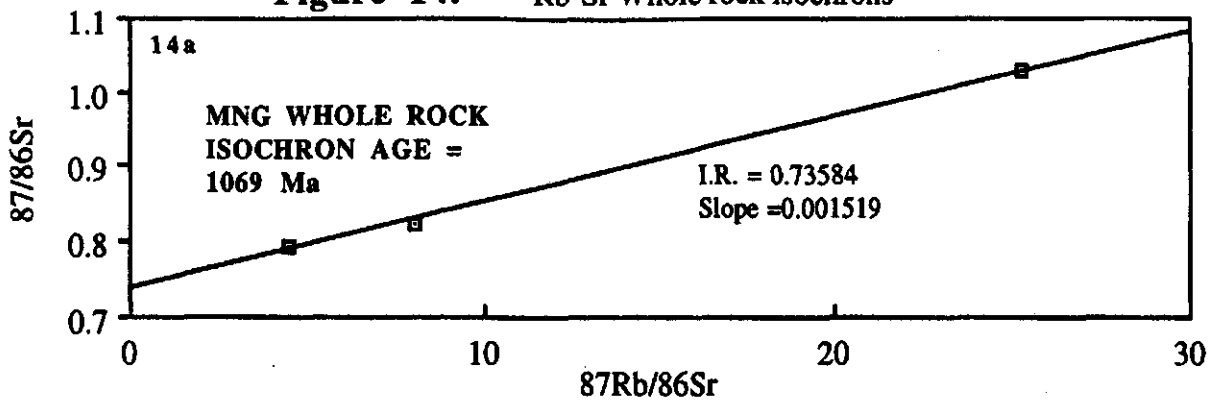

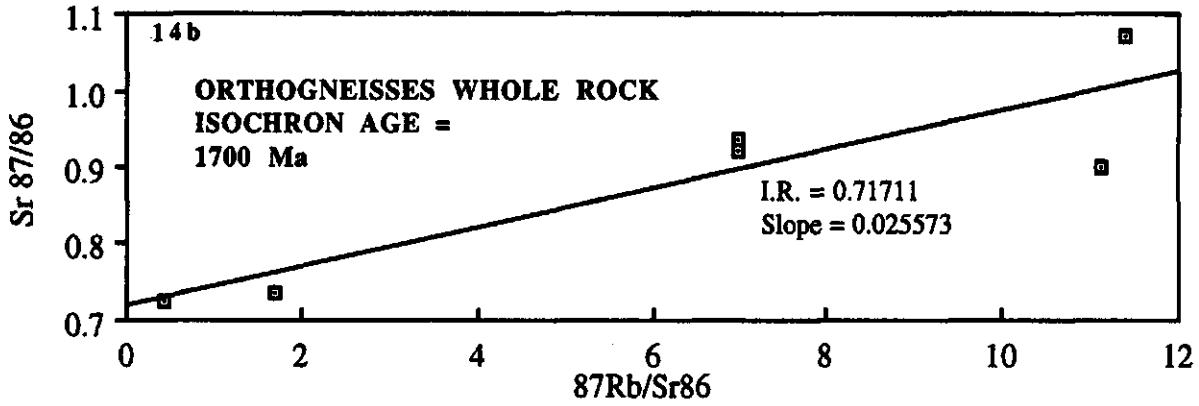

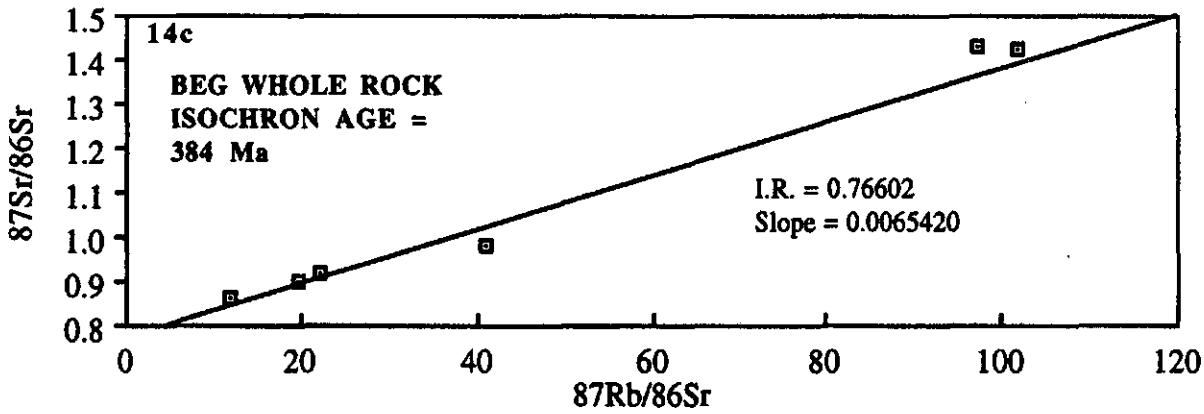

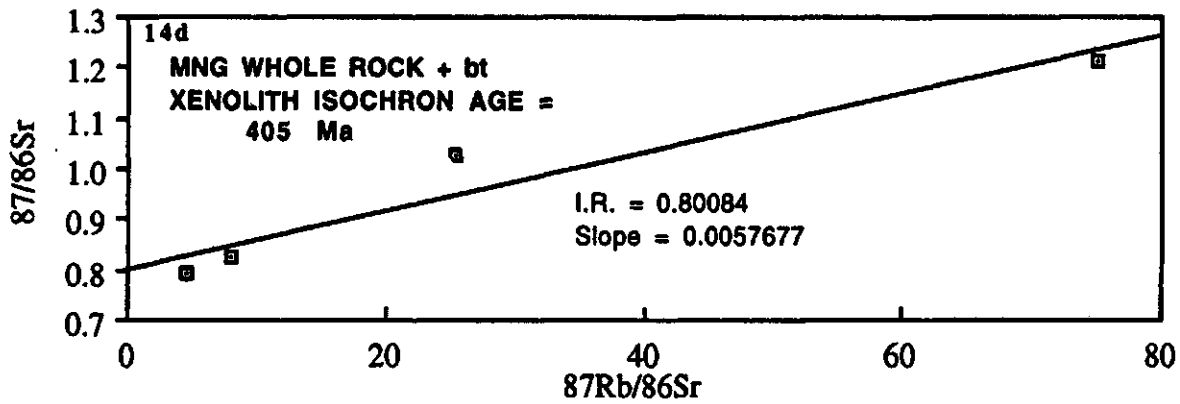

CHAPTER 5 -INTERREGIONAL CORRELATIONS FROM ISOTOPIC AND GEOCHEMICAL DATA

Looking beyond the Mt Painter and Babbage Inliers, the geochemical and isotopic data presented above offers a basis for comparison and hence correlation with surrounding terrains of similar ages.

The orthogneissic suite is distinctive by virtue of its low K_2O/Na_2O ratio (figure 13 and table 18), lower even than the Archaean of the Gawler Craton (Mortimer *et al.*, 1988) although there is a wide range of values in rocks from both regions. Wyborn *et al.* (1987) note that Australian felsic igneous suites between both 1870-1820 and 1810-1620 Ma are enriched in La, Ce, Th and U; as are the orthogneisses (figure 8 and table 2a), but K_2O values suggest a relationship with the former. In either case, the orthogneisses are more sodic than rocks of similar age. The range of model ages between 2.1 - 2.6 Ga suggests a single crustal building episode during this period, with later stage extraction of the leucocratic phases at 1.8-1.9 Ga. The orthogneisses could possibly be correlated with extensive felsic magmatism in northern Australia documented by Wyborn (1988). These felsic magmas have model ages between 2.14 - 2.34 Ga, and are found in the Arunta, Tennant Creek and Pine Creek Inliers (Wyborn, 1988). This, coupled with the similar geochemistry is indicative of penecontemporaneous felsic magmatism across Australia (Etheridge *et al.*, 1987, Wyborn, 1988).

The Mt Neill Granite displays many features in common with penecontemporaneous felsic suites in Australia (table 2a and figure 8). Most notable are high Ba values and elevated LREE, with higher K_2O/Na_2O ratios than older suites. This is consistent with values for the slightly older Hiltaba Suite Granites on the Gawler Craton (Giles, 1987) and rhyolitic units of the Older Gawler Range Volcanics (Sheard *et al.*, 1992). T_{DM} for the MNG are slightly older than that of the average Archaean - Palaeoproterozoic crust of the Gawler Craton, suggesting that the MNG was derived from hitherto unobserved Archaean material, as well as incorporating some degree of crustal mixing during magma generation.

The British Empire Granite shows similar geochemical characteristics to other Phanerozoic S-types (figure 8 and table 5), but a number of important differences may be noted. The first is that the BEG has high K_2O values and appears depleted in Fe_2O_3, CaO and MgO. The Lachlan Fold Belt S-types and the Delamerian S-type both are enriched in Ba, La, Ce, Sr and Zr relative to the BEG, which may reflect the nature of the sedimentary

Table 5: Average Whole Rock analyses comparing the Gawler Craton, Adelaide Geosyncline and Lachlan Fold Belt S-type granites with granites from the study area.

	BEG	MNG	ORTHO GNEISSES	ARCHAEAN/ PALAEOPROT	MESO- PROT.	ADELAIDEAN SEDIMENTS	DELAMERIAN S-TYPE	LFB S-TYPE GRANITES
SiO2%	76.23	66.26	70.03	62.57	65.87	60.56	71.50	70.91
Al2O3%	13.61	14.40	14.67	14.52	14.04	14.24	13.31	14.00
Fe2O3%	0.83	5.71	3.40	7.84	5.53	6.46	3.71	3.11
MnO%	0.01	0.04	0.03	0.12	0.11	0.09	0.06	0.06
MgO%	0.18	2.01	1.20	3.59	2.43	4.71	1.67	1.24
CaO%	0.32	2.09	1.72	4.3	2.65	2.15	1.84	1.88
Na2O%	2.25	3.74	4.33	2.92	2.15	1.57	2.59	2.51
K2O%	5.76	4.04	3.41	2.68	4.32	3.92	3.48	4.09
TiO2%	0.08	0.89	0.51	0.88	0.59	0.91	0.46	0.44
P2O5%	0.05	0.15	0.10	0.23	0.14	0.15	0.07	0.15
SO3%	-0.01	0.01	0.01	-	-	-	-	-
LOI%	0.69	0.59	0.48	0.76	1.76	5.06	0.54	-
TOTAL %	99.98	99.91	99.88	100.41	99.59	99.82	99.23	98.39
Al Index	1.29	1.01	1.05	0.94	1.08	1.33	1.17	1.17
K2O/Na2O	2.56	1.08	0.79	0.92	2.01	2.50	1.34	1.63
Rb ppm	365.7	349.3	241.3	90	219.9	160.1	152.2	245.0
Ba	276.0	704.0	562.4	610	637	548	596	440.0
Th	11.9	44.8	41.8	14.1	20.7	13.7	-	19.0
U	5.2	10.2	16.3	3	6.6	3.4	-	5.0
Nb	27.1	47.5	35.7	10.5	14.4	14.7	13	13.0
La	8.0	89.0	84.0	36.59	52.1	40.5	27	27.0
Ce	16.0	179.3	166.0	79.6	102.7	77.7	67	61.0
Pb	20.6	12.2	13.2	15.5	178.8	19.8	-	27.0
Sr	31.0	78.0	181.0	144.5	176.2	75.6	151.9	112.0
Nd	7.5	58.7	57.4	27.4	41.8	19.8	17.43	-
Zr	57.4	677.9	458.9	184.2	213.3	75.6	175	157.0
Sm	0.8	3.6	11.8	5.5	7.5	33.3	3.64	-
Y	29.7	145.3	93.3	27.8	40.7	204.7	53	32.0
Sc	5.6	21.3	13.3	19.3	13	15	12	11.0
Cr	16.5	17.2	13.9	262.7	141.4	109	68	30.0
V	6.7	90.4	43.7	141.3	67.3	135.8	67	49.0
Co	46.1	48.6	50.3	-	-	-	-	10.0
Ga	21.4	32.2	27.1	16.6	18.4	17.5	-	18.0
Cu	10.0	58.0	28.0	-	-	-	-	9.0
Zn	10.0	30.8	25.9	-	-	-	-	59.0
Ni	4.0	8.2	6.4	41.6	50	39	25	11.0

BEG = British Empire Granite, MNG = Mt Neill Granite.

Data for Archaean, Proterozoic, Adelaidean and Delamerian rocks from Turner *et al.* 1992, Average of 704 Lachlan Fold Belt S-types from Chappell and White, 1992.

protolith from which the BEG was derived (table 5). The Archaean model ages of the BEG suggest derivation from an unexposed sedimentary or paragneissic sequence of Archaean age or some degree of mixing similar to that discussed in 4.3 above. It appears that a combination of the two is most likely in view of the model ages obtained from the MNG.

The geochemistry of the paragneisses and the RCM are typical of ancient sedimentary sequences, and display no distinguishing characteristics. The similarity of model ages for the two units may be explained by either:

a) The two are the same unit subjected to differing degrees of metamorphism and deformation (structural arguments from field observations suggest otherwise (see 2.2.2 above)).

b) The two are sedimentary sequences of differing ages that have been sampling the same source region, or the younger has been sampling the older.

At this stage there is insufficient data available to reconcile this disparity, however in view of the rapid change of metamorphic grade and structural style over a short distance, the latter is favoured. This notion is supported by peak metamorphic temperatures obtained by Teasdale (1993) of ~450°C for the Freeling Heights Quartzite, and >650°C for the paragneissic sequence.

Other Palaeo - Mesoproterozoic sedimentary sequences in South Australia have model ages between 2.0 - 2.9 Ga (Hutchison Group, Corunna Conglomerate, Gawler Craton (Turner *et al.*, 1992)), reflecting recycling of Archaean crust, followed by a new period of crustal growth between 1.8 - 2.2 Ga, apparently coincident with Barramundi orogeny described by Etheridge *et al.* (1987). The tectonic implications of this observation are discussed in the following chapter.

CHAPTER 6 -IMPLICATIONS FOR PROTEROZOIC CRUSTAL GROWTH

6.1 Overview

The objective of the preceding work has been to establish a basis from which to discuss Proterozoic crustal growth mechanisms within the Mt Painter Inlier. From this base, incorporation of data from similar Australian terrains allows an evaluation of alternative crustal growth mechanisms thought to operate during the Proterozoic.

In the following discussion, it is essential to adopt a consistent working definition of crustal growth. New crust is therefore considered to be defined in the manner of McCulloch and Wasserburg (1978); ie, material must be derived directly from the mantle to constitute new crust, as opposed to continental growth which may incorporate recycling of pre-existing material.

This is where the Sm-Nd system becomes important, as the calculation of Nd model ages may give an age of extraction from the mantle (McCulloch & Wasserburg, 1978). Therefore, Sm-Nd model ages may be viewed as the maximum age constraint on times of addition of mantle material to the crust. This is useful in constraining periods of crustal growth.

Rb-Sr isochron ages approximate ages of crystallisation or metamorphism, closer to the 'true' stratigraphic age of a rock depending on the stability of the system (ie, if it has remained closed or not) after the formation of the rock. Rb-Sr model ages are also susceptible to resetting, resulting in correspondingly younger values that reflect metamorphism. By coupling data from the two systems and incorporating geochemical constraints, it is possible begin to delineate episodes of major crustal growth and tectonism in a specific region.

6.2 Application of Data from Hidden Valley to Crustal Growth Mechanisms

As mentioned previously, the data from Hidden Valley incorporates depleted mantle model ages (T_{DM}) that may be considered to be accurate ages of mantle extraction (as in the case of the orthogneisses and valley floor granulite) and those that are likely to have incorporated older crustal material during crystallisation, as in the case of the MNG and BEG.

Of note in the map area is that there are no model ages younger than 1.2 Ga, and when considering the depleted mantle, there are none more recent than 1.6 Ga. This

suggests that there have been no significant additions to the basement from the depleted mantle since this time. Model ages also appear to be grouped, as displayed in figure 16, at times of major crustal building activity. This phenomena is discussed below.

The map area also shows extensive evidence of crustal recycling in the form the metasedimentary sequences (both the paragneisses and Radium Creek Metamorphics) reworking older crustal material, and the subsequent derivation of magmas from this and older crustal material (eg, the S-type BEG).

Therefore, the Mt Painter Inlier offers an excellent basis from which to discuss contending hypotheses of crustal growth mechanisms.

6.3 Discussion

Opinion as to the mechanisms driving Proterozoic continental crustal growth is divided, with contention between uniformitarian and non-uniformitarian end members. On both sides there is a range of opinion, including notions that the volume of continental crust has remained steady over time (Armstrong, 1981 and 1991), or has grown in a continuous manner (Gurnis and Davies, 1986), or has in actual fact decreased (Fyfe, 1978). Workers such as Moorbath (1977) have suggested that the continental lithosphere has grown throughout earth history through episodic additions of material from the mantle. Central in all of the concepts mentioned above is the idea of an evolving mantle in response to decreasing rates of heat production and removal of more mobile elements in melts. That the mantle has evolved over time is indisputable, however the manner in which this evolution has affected the continental crust is the crux of the issue at hand.

In a steady state model such as the proposed by Armstrong (1981, and 1991), recycling of sediments on a massive scale (such as in subduction zones) is required in order to account for the geochemistry of tectonic settings that are otherwise considered to constitute the input of new mantle material (Moorbath, 1977). Large volume subduction of sediments appears difficult due to density considerations (Moorbath, 1977; McCulloch, 1987), and in view of the lack of evidence supporting modern style subduction (see below) both in the Mt Painter Inlier and Proterozoic terrains in general (Kröner, 1978), evidence for constant volume models is ambiguous at best.

Workers such as Mueller and Wooden (1988) suggest that extensive crustal recycling has been occurring for most of the history of the earth, and dominated by plate tectonic (or plate tectonic-like) processes. The question of the role of plate tectonics in continental growth is central to the debate of Proterozoic mechanisms, because in the uniformitarian viewpoint, lateral crustal growth is dominant, and the majority of new crust is formed at oceanic spreading centres. The flaw in this particular argument is the notable

absence of unambiguous ophiolites older than 800 Ma, and the lack of paired metamorphic belts in Proterozoic terrains (Kröner, 1984). For those models that suggest plate tectonics was not operating (or acting on a very localised scale) during the Proterozoic, problems arise in explaining the driving forces for orogeny and hence tectonism in the Proterozoic (McCulloch, 1987). Various models of intracontinental or "ensialic" orogeny have been offered (Etheridge *et al.*, 1987; Kröner, 1977) incorporating lithospheric underplating and subsequent crustal delamination. These are analogous to failed attempts at opening ocean basins, and explain the common features of Proterozoic orogenies that include intracontinental sedimentation and A-type magmatism. Regardless of the mechanics of such models (see Teasdale 1993 for an evaluation of modelling ensialic orogeny), all involve the input of new material from the mantle, and hence constitute continental crustal growth.

The input of new continental crustal material has been used to track the evolution of Proterozoic tectonic processes, and many workers have observed apparent peaks or 'clusters' of crustal forming activity from isotopic studies (Baer, 1983; Glikson, 1983; Moorbath, 1977) and it is often tempting to correlate these across terrains and continents, and hence imply periodic (either irregular or cyclical) mantle addition to the crust. However, caution must be exercised when doing this, as Gurnis and Davies (1986) point out that age bias from crustal recycling (regardless of mechanism or rate) is likely to result in preservation of portions of terrains of similar age, resulting in an apprent episodicity from an otherwise smoothly evolving mantle.

Data from the Mt Painter Inlier show this clustering effect, with groupings of T_{DM} around 2.0-2.4 Ga. Despite the problems associated with model ages outlined in 4.3 above, it does appear that as a range of lithologies show this age, there has been input of material from the mantle at this time. It is suggested here that the T_{DM} of the orthogneissic sequence reflects an age of mantle extrusion, resulting in the formation of a significant volume of continental crust between 2 and 2.4 Ga. Whether the orthogneisses are remnants of crust formed at this time, or later derivatives from it, is difficult to resolve. Since the T_{DM} values for the metasedimentary sequences are 2.1-2.3 Ga, sedimentation sourced from this material is implied. Cessation of sedimentation is constrained by the 1700 Ma deformational event, with another phase of sedimentation (the Radium Creek Metamorphics) beginning almost immediately and being sourced by the deformed ortho- and paragneissic sequences. This scenario adequately explains both the variation in metamorphic grade and the Nd isotopic homogeneity between the two sedimentary sequences.

Deposition of the Radium Creek Metamorphics had ceased, and a folding event taken place by the time of intrusion of the Mt Neill Granite during the earliest

Mesoproterozoic. The MNG is A-type and displays little evidence of pervasive deformation seen in older lithologies. The older (Archaean) model age for the MNG may be explained by derivation from a previously depleted deep crustal source.

A period of quiescence followed, with Adelaidean sediments being sourced from the inlier (O'Halloran 1992, Coats and Blisset 1971), consistent with a history of shallow depth of burial of the basement. Syn- or post-Delamerian Orogeny, the British Empire Granite was derived from basement sedimentary sequences, explaining the depleted trace element characteristics of this granite. The older model ages may again be explained by crustal mixing with an older source. It must be emphasised that the BEG does not represent a period of crustal growth, but rather an event incorporating the recycling of crustal material.

A possible explanation for the MNG and BEG both containing material from an older source than the orthogneissic sequence may be the juxtaposition of an Archaean crustal block adjacent to the orthogneissic source at some time after derivation of the orthogneisses. From model ages, such an Archaean block would be older than any previously recorded in South Australia, and the mechanism responsible for such a juxtaposition may reflect the tectonic processes acting between the time of derivation of the orthogneisses (no older than 2.4 Ga) and the time of derivation of the Mt Neill Granite (no younger than 1.6 Ga).

Tectonic activity within the Mt Painter Inlier has continued throughout the Phanerozoic, with sufficient uplift to allow sourcing of Mesozoic sediments, and continued faulting and thrusting throughout the Tertiary. It is this latest (and still continuing) phase of faulting that is responsible for the present day morphology of the inlier as a whole, and the topography of Hidden Valley.

One obvious problem with a major crustal forming event at 2.1-2.4 Ga is the absence of outcropping lithologies of this age. The orthogneisses may themselves be of this age, however contact relationships with the paragneisses and Rb-Sr data suggest a pre-syn-orogenic timing at ~1700 Ma. Alternatively, the cluster of model ages obtained 2.1-2.4 Ga may instead reflect an average age that is the result of mixing of older (Archaean) crust with newly derived material from the mantle, as in the case of the MNG. In such a scenario, the period from 2.1-2.4 Ga would not reflect the addition of any new material to the crust at all, and would in effect be a result of the sampling and calculation process. Unfortunately, due to time constraints it has not been possible to calculate the % mixing between the depleted mantle and an Archaean crustal component necessary to produce model ages such as those observed within the map area.

6.4 Conclusions and recommendations

To summarise, continental crustal growth in the Mt Painter Inlier may be resolved to a crustal forming event from 2.0 to 2.4 Ga, the orthogneisses being either remnants of the crust formed during this event or derived directly from this material at a later stage. Subsequent continental growth in the inlier has involved recycling processes, specifically sedimentation and the derivation of magmas from sediments and previously depleted lower crust. The MNG and BEG are sourced from a terrain that is ~3 Ga, and the derivation of these magmas subsequent to the extraction of the orthogneisses suggests a major change in the terrain being sampled by the magmas. Therefore, the MNG and BEG do not represent the input of new crustal material at the times of their crystallisation, but sampling of Archaean crustal material that was not in physical proximity to the inlier at the time of extraction of the orthogneisses.

In the global context, the Mt Painter Inlier displays the hallmarks of typical Proterozoic orogeny, including intracontinental sedimentation and syn- or rapidly post-orogenic A-type magmatism. There is no evidence of modern style plate tectonism associated with orogenesis during the Proterozoic in the Mt Painter Inlier. The evidence therefore supports the notion of a non-uniformitarian mechanism of tectonism and orogeny involving the input of new crustal material from the mantle. However, questions as to the nature and origin of the driving forces of such ensialic orogeny remain unanswered, and only further study will further elucidate such problems.

Possible further investigations within the Mt Painter Inlier would of necessity include:

a) Extensive geochemical and isotopic (specifically Sm-Nd and U-Pb) work within the orthogneissic sequence to delineate stratigraphy, timing of mantle additions and crystallisation ages.

b) igneous petrology of the Mt Neill Granite to elucidate source characteristics, lithological heterogeneity and comparative geochemistry with the Pepegoona Porphyry. U-Pb crystallisation ages and a study of the igneous fabrics would also be important.

c) determination of an accurate crystallisation age of the British Empire Granite.

d) investigation into the structural and metamorphic characteristics of metasedimentary sequences to the north of Hidden Valley, specifically the Brindana Schist. Supporting isotopic work (Sm-Nd) is a must.

e) study of the valley floor melange (particularly the matrix) in order determine unambiguously the origin of Hidden Valley. This is central to developing an understanding of the tectonic evolution of the inlier.

f) collation and correlation of drill hole data from basement intersections from the plains to the east.

and g), investigations into the nature of the regional gravity low beneath the inlier may shed some light on Phanerozoic tectonic processes.

To conclude, this study has shown that the Mt Painter Inlier offers an excellent opportunity for investigations into the nature of Proterozoic tectonism. Preliminary results suggest a period of crustal growth at ~2.0-2.4 Ga, and that ensialic orogeny has been active in the province. However, investigations of this nature are still in their infancy, and the potential for future multidisciplinary studies into Proterozoic continental growth processes is immense.

ACKNOWLEDGEMENTS

This project has been the result of the efforts of a large number of people, without whom none of this would have been possible. Firstly, thanks to my supervisors John Foden and Mike Sandiford for conceptualisation of the project and critical evaluation of data and interpretations as they came to hand. Thanks too to Jon Teasdale for putting up with me in the field, for his insight into the structural complexities of the area and the thankless hours put into production of the map.

Fieldwork was made possible through the use of vehicles supplied and fuelled by SADME, and thanks must go to Malcom Sheard for follow up discussions. Also a big thankyou to those involved in trying to get the map to print, but it was destined not to be! Thanks must also go to CRA for supplying base maps, aeromag data and helicopter support.

The crew at Arkaroola made fieldwork a memorable experience, particularly radio scheds. and Wednesday nights. Thanks Bruce and Marley, the blokes from Monash, and to all the staff at Arkaroola for the warm welcome and good times.

Analysis of the samples was made easier for the good humour of the analytical staff, particularly David Bruce (who I'm sure was convinced that I'd never finish my isotopes), Mary Jane (who ploughed on until the job was done... thanks for the numbers), John Stanley and Phil McDuie (for advice related to troublesome fused disks), Geoff Trevelyn and any others who had some input on analysis.

During writing, much help and advice has come from a number of people, but a big thankyou to all of the other honours students for peaking out, going mad and occasionally offering suggestions, all at (in)appropriate times. Particulary those in our office and fellow igneous students (Scotty, Deano and Mandy) as well as Danni, John, Peta and Wade.

Finally, for preventing me from going completely mad during the year, thanks to Mum and Dad for living 500 kms away, also thanks to Rachel for being there at the end.

REFERENCES

Allegre, C.J. and Rousseau, D., 1984. The growth of the continents through geological time; studies by Nd isotope analysis of shales. *Earth Planet. Sci. Lett.*, **67**, p. 19-34.

Armstrong, R.L., 1981. Radiogenic isotopes: The case for crustal recycling on a near-steady-state no-continental-growth Earth. *Philos. Trans. R. Soc. London, Ser. A*, **301,** p. 443-472.

Armstrong, R.L. 1991. The persistent myth of continental growth. *Aust. Jl. Earth Sc.* **38**, p.613-630.

Baer, A.J. 1983. Proterozoic orogenies and crustal evolution. *In*: *Geological Society of America.* **Memoir 161,** p. 47-58.

Benton, J.S. 1993. A sedimentological and isotope investigation into the provenance and depositional setting of Palaeo- and Neoproterozoic sediments in the Mt Painter Inlier. Hon. Thesis, Univ. of Adel. (Unpubl.).

Black, L.P. and McCulloch, M.T. 1984. Sm-Nd ages of the Arunta, Georgetown and Tennant Creek Inliers of Northern Australia. *Aust. Jl. Earth Sc.* **31**, p. 49-60.

Blight, P.G. 1977. Uraniferous metamorphics and "Younger" granites of the Paralana area, Mount Painter Province, South Australia: A Petrographical and geochemical study. Hons. Thesis, Univ. of Adel. (Unpubl.).

Coats, R.P. and Blisset, A.H. 1971 Regional and economic geology of the Mount Painter Province. South Aust. Dept. Mines and Energy. **Bull 43.**

Chappell, B.W. and White, A.J.R. 1992. I- and S-type granites in the Lachlan Fold Belt. *Trans. Royal Soc. Edinburgh.* **83,** p. 1-26.

Creaser, R.A. and White, A.J.R. 1991. Yardea Dacite- Large volume, high - temperature felsic volcanism from the Middle Proterozoic of South Australia. *Geology,* **19,** p.48-51.

DePaolo, D.J., Linn, A.M. and Schubert, G. 1991. The continental crustal age distribution: Methods of determining mantle separation ages from Sm-Nd isotopic data and application to the Southwestern United States. *Jl. Geophys. Res.* **96 B2,** p. 2071-2088.

DePaolo, D.J. and Wasserburg, G.J. 1976. Inferences about magma sources and mantle structure from variations of $^{143}Nd/^{144}Nd$. *Geophys. Res. Lett.* **3,** p: 743-746.

Etheridge, M.A., Rutland, R.W.R. and Wyborn, L.A.I. 1987. Orogenesis and tectonic process in the early to middle Proterozoic of northern Australia. *In*: Proterozoic Lithospheric Evolution, *Am. Geophys. Union Geodyn. Ser.*, **17**, p.131-147.

Fletcher, I.R., Paul, D.K. and Trendall, A.F. 1992. Sm-Nd and geochemical characteristics of metasedimentary rocks at Mt. Narryer, Western Australia. *Aust. Jl. of Earth Sc.* **39**, p. 67-78.

Fyfe, W.S. 1978. The evolution of the Earth's crust: modern plate tectonics to ancient hot spot tectonics? *Chemical Geology* **23**, p. 89-114.

Giles, C.W. 1988. Petrogenesis of the Proterozoic Gawler Range Volcanics, South Australia. *Precambrian Res.* **40/41,** p. 407-427.

Glikson, A.Y. 1983. Geochemical, isotopic, and palaeomagnetic tests of early sial-sima patterns: The Precambrian crustal enigma revisited. *In*: *Geological Society of America.* **Memoir 161,** p. 95-117.

Goldstein, S.L. 1988. Decoupled evolution of Nd and Sr isotopes in the continental crust and the mantle. *Nature* **336**, p. 733-738.

Gurnis, M. and Davies, G.F., 1986. Apparent episodic crustal growth arising from a smoothly evolving mantle. *Geology.* **14**, p. 396-399.

Hoffman, P.F., 1980. A Wilson cycle of early Proterozoic age in the northwest of the Canadian Shield. *In:* The Continental Crust and its Mineral deposits. Ed. by D.W. Strangway. *Geol. Assoc. Can.* **Spec. Paper 20**, p.523-549.

Jacobsen, S.B., 1988. Isotopic constraints on crustal growth and recycling. *Earth Planet. Sci. Lett.* **90**, p.315-329.

Kröner, A., 1977. Precambrian mobile belts of southern and eastern Africa - ancient sutures or sites of ensialic mobility? A case for crustal evolution towards plate tectonics. *Tectonophysics* **40**, p. 101-135.

Kröner, A., 1984. Evolution, growth and stabilisation of the Precambrian lithosphere. *In:* Structure and Evolution of the Continental Lithosphere. *Ed.* H.N. Pollack and U.R. Murthy, Physics of the Earth, **15,** p. 69-106.

McCulloch, M.T., and Wasserburg, G.J., 1978. Sm-Nd and Rb-Sr chronology of continental crust formation. *Science*, **200**, p. 1003-1011.

McCulloch, M.T., 1987. Sm-Nd isotopic constraints on the evolution of Pre-Cambrian crust in the Australian continent, *In*: Proterozoic Lithospheric Evolution, *Am. Geophys. Union Geodyn. Ser.*, **17**, p. 115-130.

Mildren, S.D., 1992. Heat Refraction and the Metamorphic Process: Calculations, with applications to unconformity - related contact metamorphism in the Northern Flinders Ranges. Hons. Thesis, Univ. Adel. (Unpubl.).

Moorbath, S. 1977. Ages, isotopes, and evolution of Precambrian continental crust. *Chemical Geology* **20**, p. 151-187.

Moores, E.M. 1986. The Proterozoic ophiolite problem, continental emergence, and the Venus connection. *Science,* **234**, p.65-68.

Moores, E.M. 1993. Neoproterozoic oceanic crustal thinning, emergence of continents, and origin of the Phanerozoic ecosystem: A model. *Geology,* **21** p. 5-8.

Mortimer, G.E., Cooper, J.A. and Oliver, R.L. 1988. The geochemical evolution of Proterozoic granitoids near Port Lincoln in the Gawler orogenic domain of South Australia. *Precamb. Res.* **40/41,** p. 387-406.

Mueller, P.A. and Wooden, J.L. 1988. Evidence for Archaean subduction and crustal recycling, Wyoming province. *Geology* **16,** p. 871-874.

O'Halloran, G, 1992. The evolution of provenance and depositional processes during early Adelaidean sedimentation. A sedimentological and Nd isotope investigation. Univ. Adel. Hons. Thesis. (Unpubl.)

Page, R.W. 1985. Isotopic record of Proterozoic crustal events in Northern Australia. *In*: Abstracts for the tectonics and geochemistry of Early - Middle Proterozoic Fold Belts, Darwin 1985. *Bureau Mineral Resources, Geology & Geophysics, Record* 1985/28.

Parker, A.J., Fanning, C.M., Flint, R.B., Martin, A.R. and Rankin, L.R. 1988. Archaean - Early Proterozoic granitoids, metasediments and mylonites of southern Eyre Peninsula, South Australia. *Specialist Group in Tectonics and Structural Geology Field Guide Series No. 2.* GSA.

Pearce, J.A., Harris, N.B.W., and Tindle, A.G. 1984. Trace element discrimination diagrams for the tectonic interpretation of granitic rocks. *Jl. of Petrology,* **25 part 4,** p.956-983.

Roberts, R.H. 1976. Structure and petrology of basement metasediments and granites in the Mount Painter Inlier. Hons. Thesis, Univ. of Adel. (Unpubl.).

Roberts, M.P. and Clemens, J.D. Origin of high-potassium, calc-alkaline, I-type granitoids. *Geology*. **21**, p. 825-828.

Rutland, R.W.R., 1982. On the growth and evolution of continental crust: a comparative tectonic approach. *Jl. Proc. R. Soc. NSW.* **115**, p.33-60.

Shaw, D.M., 1980. Evolutionary tectonics of the Earth in light of early crustal structure. In: The Continental Crust and its Mineral deposits. Ed. by D.W.Strangway. *Geol. Assoc. Can.* **Spec. Paper 20**, p.66-73.

Sheard, M.J., Fanning, C.M. & Flint, R.B. 1992. Geochronology and definition of Mesoproterozoic volcanics and granitoids of the Mt Babbage Inlier, northern Flinders Ranges. *Geological Survey of South Australia.Quarterly Geological Notes,* **123,** p. 18-32.

Smith, A.D. and Ludden, J.N. 1989. Nd isotopic evolution of the Precambrian mantle. *Earth Plan. Sc. Lett.* **93**, p.14-22.

Sun S-s, and McDonough, W.F., 1989. Chemical and isotopic systematics of ceanic basalts: implications for mantle composition and processes. *In:* Saunders, A.D. and Norry, M.J. (eds.) Magmatism in the ocean basins. *Geol. Soc. Spec. Publ.* **42,** p. 313-345.

Taylor, S.R. and McLennan, S.M. 1983. Geochemistry of Early Proterozoic sedimentary rocks and the Archaean/Proterozoic boundary. *In*: *Geological Society of America.* **Memoir 161,** p. 119-131.

Teale, G.S. 1979. Revision of nomenclature for Palaeozoic intrusives of the Mt Painter Province, South Australia. *Trans. Royal Soc. S.A.* **103,** p. 95-100.

Teale, G.S. 1993. The Nooldoonooldoona Trondjemite and other newly recognised Mesoproterozoic intrusives of the Mt Painter Province. *Geological Survey of South Australia. Quarterly Geological Notes,* **125,** p 20-31.

Teale, G.S., (*in press*) a. Palaeoproterozoic of the Mount Painter and Mount Babbage Inliers. *In*: Geology of South Australia.*Geological Survey of South Australia. Bulletin.*

Teale, G.S., (*in press*) b. Mesoproterozoic of the Mount Painter and Mount Babbage Inliers. *In*: Geology of South Australia. *Geological Survey of South Australia. Bulletin.*

Teasdale, J.P. 1993. Proterozoic tectonic models with applications to the Mount Painter Inlier. Univ. Adel. Hons. Thesis (Unpubl.).

Turner, S.P., Foden, J.D. and Morrison, R.S. 1990. Derivation of some A-type magmas by fractionation of basaltic magma: An example from the Padthaway Ridge, South Australia. *Lithos.* **28,** p.151-179.

Turner, S.P., Foden, J.D., Sandiford, M. and Bruce, D. 1992. Sm-Nd isotopic evidence for the provenance of sediments from the Adelaide Fold Belt and southeastern Australia with implications for episodic crustal addition. *Geochim. et Cosmo. Acta.* **57,** p. 1837-1856.

Webb, A.W. 1976. Geochronology. *In*: Radke, F. & Webb, A.W. Geochronology of the eastern basement rocks. Amdel progress reports 9 and 10. *South Australia. Department of Mines and Energy. Open File Envelope,* 2136. (Unpubl.)

West, G.F., 1980. Formation of continental crust. In: The Continental Crust and its Mineral deposits. Ed. by D.W. Strangway. *Geol. Assoc. Can.* **Spec. Paper 20**, p.117-148.

Wetherly, S., 1991. Constraints on Proterozoic tectonics: Theoretical calculations and an example from the Entia Gneiss Dome, Central Australia. Hons. Thesis, Univ. Adelaide. Unpub.

Whalen, J.B., Currie, K.L. & Chappell, B.W. 1987. A-type granites: geochemical characteristics, discrimination and petrogenesis. *Contrib. Min. Petr.* **95,** p. 407-419.

Windley, B.F., 1981. Precambrian rocks in the light of the plate tectonic concept. *In:* Precambrian Plate Tectonics. *Ed.* A. Kroner. p. 1-20.

Wyborn, L.A.I., 1985. Geochemistry and origin of a major Early Proterozoic felsic igneous event of Northern Australia and evidence for substantial vertical accretion of the crust. *In*: Abstracts for the tectonics and geochemistry of Early - Middle Proterozoic Fold Belts, Darwin 1985. *Bureau Mineral Resources, Geology & Geophysics, Record* 1985/28.

Wyborn, L.A.I., 1988. Petrology, geochemistry and origin of a major Australian 1880-1840 Ma felsic volcano-plutonic suite: A model for intracontinental felsic magma generation. *Prec. Res.* **40/41,** p. 37-60.

Wyborn, L.A.I., Page, R.W. and Parker, A.J. 1987. Geochemical and geochronological signatures in Australian Proterozoic igneous rocks. *From*: Pharaoh, T.C., Beckinsale, R.D. & Rickard, D. (eds) 1987, *Geochemistry and Mineralisation of Proterozoic Volcanic Suites,* Geological Society Special Publication **No. 33,** p 377-394.

APPENDIX A:

SELECTED THIN SECTION DESCRIPTIONS

All samples are prefixed A1015-

APPENDIX A: SELECTED THIN SECTION DESCRIPTIONS

HV-11: Freeling Heights Quartzite, North end of Valley

Mineralogy:	Quartz:	60%
	Muscovite:	30%
	Saussurite:	5%
	Opaques:	10%

H.S. Light brown- yellow brown micaceous quartzite. Well developed schistosity.

T.S. Aligned massive quartz-mu fabric. Prominent weathering effects, however this is interpreted to be a facies variation of the massive quartzite found further south (HV-55).

HV-12: Mt Neill Granite

Mineralogy:	Quartz:	35%
	Microcline:	45%
	Sphene:	5%
	Clay minerals:	<10%

H.S. Euhedral feldspar crystals <10mm in size, supported in a fine grained, brick red matrix.

T.S. Textures: Microcline appears as late stage, cutting across qtz. No evidence of any type of metamorphic fabric, however irregular grain boundaries suggest some degree of retrogression or alteration.

HV-18: Feldspathic Quartzite in Valley Fill

Mineralogy:	Quartz:	80%
	Biotite:	15%
	Plagioclase:	15%
	?sillimanite:	8%
	Opaques:	2%

H.S. Medium grain size, pinky-grey quartzite, cm scale laminations suggest bedding.

T.S. Alternating quartz rich and biotite+?sill rich layers suggest sedimentary processes. Possible D_2 fabric suggested by subtle alignment of larger biotite grains. Biotite contains zircons.

HV-40: Corundum Schist

Mineralogy:	Muscovite:	80%
	Quartz:	15%
	Corundum:	5%

H.S. Yellow-brown-green to khaki schist with large (3-4cm) hexagonal crystals containing dark blue corundum in their cores. Dominant schistose fabric, commonly also contains crenulations.

T.S. Textures: Large muscovite crystals occasionally contain opaques along cleavage, supported in very fine grained (?muscovite) groundmass. Quartz grains display undulose extinction.

HV-41: Granulite, Valley Floor

Mineralogy:	Olivine:	30%
	Plagioclase:	30%
	Orthopyroxene:	10%
	Spinel:	15%
	Ti- hornblende:	10%
	Serpentine:	5%

H.S. Dense dark matrix containing aligned feldspar crystals (<0.5cm).

T.S. Textures: Abundant sp-opx symplectites, optical continuity between opx crystals and opx in symplectites. Olivine has retrograded to serpentine, resulting in a volume increase and radial fractures emanating from olivine grains. Plagioclase displays a preferred alignment.

HV-55: Freeling Heights Quartzite

Mineralogy:	Quartz:	65%
	Muscovite:	30%
	Opaques:	5%
	Plagioclase:	<1%

H.S. Light brown massive quartzite.

T.S. Textures: Blocky equigranular quartz grains, occasional triple junctions. Muscovite occurs as discrete grains that are aligned sub-parallel.

HV-56: British Empire Granite

Mineralogy:	Quartz:	35%
	Plagioclase:	30%
	Microcline:	25%
	Muscovite:	10%

H.S. Medium to coarse grained white granite containing randomly oriented muscovite flakes.

T.S. Textures: Randomly oriented muscovite flakes supported in a qtz-plag-micro groundmass. Rare mu grains appear to be rimmed by clays, suggesting very recent alteration .

HV-65: Pink Granite Gneiss

Mineralogy:	Quartz:	35%
	Microcline:	30%
	Biotite:	15%
	Opaques:	10%
	Allanite:	<5%
	Undifferentiated:	<5%

H.S. Pinky red quartzofeldspathic gneiss containing a fabric defined by bt wrapping around qtz+fspar ?augen.

T.S. Textures: Preferential growth of opaques in bt, possibly reflecting a retrograde event. Also symplectites (?qtz-fspar) and spotty textures within the microcline and quartz grains displaying undulose extinction, suggesting a pervasive metamorphic overprinting.

HV-67: Red Granite Gneiss

Mineralogy:	Quartz:	45%
	Microcline:	45%
	Allanite:	5%
	Biotite:	<5%

H.S. Red granite gneiss with large allanite crstals surrounded by paler coloured rims. Contains foliation typical of orthogneissic sequence.

T.S. Allanite crystals are hollowed within and are surrounded by clay rims (possibly due to weathering of radioactive halo). There appears to be two phases of quartz; one highly strained and a later stage displaying only slight undulose extinction. The former also show a subtle S-C fabric.

HV-74: Troctolite

Mineralogy:	Spinel:	30%
	Olivine:	30%
	Plagioclase:	30%
	Serpentine:	10%

H.S. Dense black and white gabbro, suggestion of alignment of feldspars.

T.S. Symplectites around olivine of spinel that is optically continuous. Volume expansion retrogression around olivine with the production of serpentine, resulting in the formation of a radial fracture pattern originating from the olivine.

HV-78: Yagdlin Phyllite

Mineralogy:	Quartz:	40%
	?muscovite:	35%
	Almandine:	15%
	Opaque porphs:	10%

H.S. Mauve- light pink phyllite displaying alternating light and dark bands (?bedding) that are folded. Also present is an axial planar foliation.

T.S. Textures: The porphyroblasts occur in bands at a low angle to 'bedding', and the porphyroblasts are generally prismatic. A very fine grained groundmass (?mu) occasionally appears crenulated parallel to 'bedding'.

Almandine is late stage and cross cuts existing fabrics, and are themselves commonly rimmed with a deep red-brown coloured fringe.

HV-81: Sillimanite Gneiss

Mineralogy:	Quartz:	40%
	Microcline:	20%
	Sillimanite:	10%
	Biotite:	<10%
	Muscovite:	<10%
	Opaques:	<10%

H.S. Light brown to yellowish micaceous gneiss.. quartz appears to have been recrystallised.

T.S. Textures: Sill occurs as fibrolite, and defines a fabric that wraps around qtz grains, but also appears to as fine splays within some grains. The sill also appears to be intimately related with mu.

HV-84: Leucogranite gneiss

Mineralogy:	Quartz:	45%
	Plagioclase:	25%
	Microcline:	20%
	Biotite:	10%

H.S. White igneous rock containing occasional bt grains that appear oriented sub-parallel.

T.S. Textures: Qtz-plag symplectites, with many plag grains appearing to be saussurised. The qtz grains exhibit signs of strain in the form of undulose extinction and an indistinct preferred orientation.

APPENDIX B:

TABLES OF WHOLE ROCK ANALYSES

All samples are prefixed A1015-; except those
prefixed 948-92- and 92-2-

APPENDIX B

	BEG					MNG					
	948-92-BE1	948-92-BE2	948-92-BE3	948-92-BE4	HV-56	92-2-1A	92-2-1B	HV-12	HV-13*	HV-29	HV-32
SiO2%	75.25	77.10	76.19	76.56	77.20	68.76	68.49	75.07	36.78	60.58	69.91
Al2O3%	13.19	12.84	13.30	13.04	14.03	14.88	14.67	14.29	17.72	16.41	14.20
Fe2O3%	1.18	0.49	0.57	0.19	0.47	4.30	5.06	0.87	9.09	7.08	3.79
MnO%	0.01	0.02	0.02	0.00	0.01	0.03	0.03	0.00	0.04	0.09	0.01
MgO%	0.23	0.14	0.14	0.08	0.12	0.28	0.37	0.18	18.99	0.68	1.27
CaO%	0.04	0.50	0.56	0.48	0.60	1.33	1.26	0.19	0.29	3.10	0.09
Na2O%	0.23	3.21	3.29	3.14	4.27	4.34	4.35	5.61	0.37	2.71	2.04
K2O%	8.31	4.52	4.66	5.59	3.20	4.88	4.56	3.26	9.08	6.91	6.71
TiO2%	0.12	0.05	0.06	0.03	0.04	0.41	0.44	0.40	1.40	0.91	0.49
P2O5%	0.05	0.10	0.09	0.07	0.04	0.07	0.07	0.05	0.22	0.25	0.05
SO3%'	0.00	0.00	0.00	0.00	-0.01	0.02	0.03	0.00	0.00	0.00	0.00
LOI%	0.85	0.47	0.49	0.26	0.52	0.37	0.58	0.36	1.07	0.17	0.82
TOTAL	99.46	99.44	99.37	99.44	100.49	99.67	99.91	100.28	95.05	98.89	99.38
Rb	499.0	293.8	327.6	250.3	232.4	206.2	200.4	112.0	952.1	366.1	311.9
Ba	460.0	152.0	317.0	241.0	92.0	801.0	772.0	309.0	620.0	1781.0	573.0
Th	19.0	8.8	10.2	10.4	4.8	62.8	64.5	81.6	32.6	-2.1	82.3
U	6.3	24.8	14.9	15.7	4.0	20.8	20.5	18.4	10.6	-0.8	9.5
Nb	28.5	19.4	20.2	4.5	25.6	41.6	47.8	62.9	60.9	42.7	60.3
K	68985.4	37522.7	38684.9	46405.3	26564.8	40511.3	37854.8	27062.8	75377.5	57363.3	55703.0
La	13.0	10.0	8.0	7.0	3.0	148.0	152.0	93.0	137.0	39.0	81.0
Ce	25.0	21.0	15.0	13.0	7.0	281.0	297.0	188.0	252.0	91.0	187.0
Pb	22.2	22.7	24.3	27.2	18.9	19.6	14.2	7.0	2.7	19.2	18.6
Sr	35.1	38.3	47.6	61.5	26.8	76.9	88.8	37.5	33.9	136.5	20.3
P	218.2	436.4	392.8	305.5	174.6	305.5	305.5	218.2	960.1	1091.1	218.2
Nd	9.0	8.0	5.0	5.0	6.0	125.0	129.0	14.9	12.4	59.0	96.0
Zr	69.4	38.3	37.4	28.6	45.4	545.2	580.2	639.2	428.6	1308.2	864.3
Sm					0.8			3.9	3.4		
Tl	719.4	299.7	359.7	179.8	239.8	2457.9	2637.8	2398.0	8393.0	5455.4	2937.5
Y	36.1	31.7	32.6	21.8	23.3	125.4	126.7	164.1	331.4	50.8	134.3
Sc	6.0	3.4	4.0	1.8	5.1	6.1	7.7	2.1	44.6	18.8	8.1
Cr	29.0	31.0	29.0	29.0	4.0	3.0	1.0	2.0	18.0	-1.0	2.0
V	8.2	4.4	5.1	3.8	5.2	3.2	3.2	2.3	218.8	5.3	2.6
Co	35.2	30.1	44.4	35.9	57.0	48.5	26.0	78.3	22.6	51.6	47.5
Ga	19.6	17.4	18.0	14.8	23.1	27.2	27.8	22.9	51.7	32.8	31.9
Cu	13.0	0.0	2.0	-1.0	7.0	10.0	9.0	11.0	4.0	11.0	157.0
Zn	8.0	11.0	10.0	4.0	12.0	45.0	36.0	10.0	21.0	76.0	9.0
Ni	3.0	4.0	-2.0	2.0	5.0	-2.0	2.0	3.0	14.0	7.0	8.0

* = samples that returned poor totals (<98.5%) after initial measurement were reweighed, ignited and fused. This made no difference to the totals, suggesting problems due to OH in micas or high levels of unmeasured elements (eg F, Cl).

APPENDIX B

			ORTHOGNEISSE							
HV-48	HV-57	HV-72	92-2-2	HV-60*	HV-84	BET-1	BET-2	92-2-3	HV-59	HV-87
75.86	70.52	51.31	72.51	67.87	73.54	72.44	70.03	68.52	77.96	74.95
13.35	14.28	14.21	15.01	17.09	14.46	16.11	15.42	13.62	13.16	13.60
0.82	3.77	13.86	1.46	1.71	1.54	1.53	2.77	7.43	0.41	2.65
0.01	0.01	0.11	0.02	0.01	0.03	0.02	0.05	0.03	0.00	0.01
1.31	0.32	6.30	0.57	0.57	0.54	0.53	1.01	0.89	0.06	0.33
0.27	0.23	6.73	2.14	3.24	1.79	3.20	2.43	0.36	0.19	0.15
6.28	3.22	2.97	4.29	5.48	3.68	5.07	3.34	6.37	6.93	7.35
1.00	5.93	1.29	3.28	1.16	3.95	1.19	4.00	0.69	0.31	0.11
0.37	0.51	2.26	0.19	0.18	0.20	0.20	0.44	0.62	0.05	0.18
0.06	0.09	0.43	0.06	0.09	0.05	0.06	0.14	0.13	0.02	0.03
-0.01	0.00	0.00	0.01	0.00	0.00	0.00	0.00	0.04	-0.01	-0.01
0.47	0.86	0.82	0.23	0.33	0.28	0.16	0.49	0.83	0.36	0.43
99.79	99.76	100.30	99.77	97.72	100.05	100.49	100.14	99.53	99.44	99.78
88.2	429.8	147.7	155.9	77.4	186.1	103.2	210.2	57.1	19.1	5.7
148.0	574.0	140.0	616.0	146.0	450.0	192.0	776.0	93.0	39.0	19.0
92.1	117.2	11.8	1.5	2.1	11.7	1.9	8.6	451.8	9.7	177.1
14.9	126.5	2.6	1.2	1.3	3.9	1.4	2.2	71.5	2.8	68.4
32.2	62.7	16.5	12.0	12.3	6.9	9.1	17.6	60.9	6.9	40.9
8301.5	49227.8	10708.9	27228.9	9629.7	32790.9	9878.8	33205.9	5728.0	2573.5	913.2
101.0	248.0	36.0	3.0	12.0	27.0	14.0	35.0	495.0	7.0	118.0
200.0	485.0	77.0	7.0	13.0	44.0	23.0	56.0	882.0	12.0	229.0
9.0	11.3	5.9	14.0	17.3	15.8	13.7	20.4	21.2	2.8	13.6
56.4	46.7	162.6	398.3	534.8	312.7	489.8	306.4	28.2	41.0	26.0
261.9	392.8	1876.6	261.9	0.0	218.2	261.9	611.0	567.3	87.3	130.9
34.2	136.9	45.0	3.0	3.8	24.0	13.0	23.0	279.0	7.0	88.0
321.2	637.7	282.1	107.5	120.9	112.7	90.2	211.9	656.8	51.3	257.1
7.0	32.9			0.8						
2218.1	3057.4	13548.7	1139.0	1079.1	1199.0	1199.0	2637.8	3716.9	299.7	1079.1
97.1	147.2	65.5	8.9	12.4	14.3	14.2	12.5	156.6	22.8	101.2
7.6	8.0	48.3	5.6	56.0	3.7	5.7	6.2	9.8	0.9	1.6
8.0	2.0	79.0	20.0	8.0		11.0	16.0	-17.0	3.0	4.0
22.5	7.2	310.1	17.2	18.8	19.0	21.8	34.5	23.5	5.3	11.7
67.1	81.9	42.9	30.0	33.4	37.4	48.2	35.6	31.8	83.1	45.4
27.1	29.7	26.6	18.8	26.1	21.6	22.6	24.3	25.8	18.5	26.4
10.0	19.0	155.0	3.0	10.0	5.0	9.0	7.0	106.0	11.0	8.0
7.0	25.0	24.0	20.0	19.0	33.0	34.0	51.0	16.0	8.0	9.0
5.0	5.0	19.0	4.0	10.0	11.0	8.0	13.0	3.0	4.0	7.0

* = samples that returned poor totals (<98.5%) after initial measurement were reweighed, ignited and fused. This made no difference to the totals, suggesting problems due to OH in micas or high levels of unmeasured elements (eg F, Cl).

APPENDIX B

S							PARAGNEISSES			
HV-66	HV-79*	HV-80	HV-86	HV-65	92-2-4	92-2-8	948-92-FHQ1	948-92-FHQ2	HV-50*	HV-58
64.85	63.10	71.34	66.24	70.68	68.76	73.06	84.10	84.12	65.59	92.70
14.28	12.86	13.16	15.16	12.79	14.77	15.68	7.42	8.42	10.25	3.70
8.09	8.63	4.66	6.03	4.44	2.98	0.95	2.16	2.04	6.81	1.58
0.11	0.11	0.05	0.05	0.02	0.02	0.02	0.03	0.01	0.06	0.02
1.28	0.91	0.42	0.74	1.01	2.66	0.50	1.87	0.34	7.65	0.36
3.34	3.67	1.61	2.46	0.43	0.43	2.64	0.01	0.06	0.23	0.03
3.53	2.24	2.65	3.81	1.83	6.21	5.51	0.14	0.12	1.03	0.27
2.31	4.69	5.11	3.74	7.43	2.17	1.01	2.75	2.73	4.76	1.26
1.05	0.84	0.48	0.54	0.59	0.60	0.15	0.27	0.27	0.72	0.10
0.25	0.17	0.07	0.12	0.07	0.12	0.03	0.01	0.05	0.06	0.01
0.00	0.01	0.00	0.00	0.00	0.02	0.02	0.00	0.00	0.00	-0.01
0.40	0.38	0.16	0.56	0.37	0.54	0.35	0.91	1.13	0.86	0.47
99.49	97.61	99.71	99.46	99.67	99.28	99.92	99.67	99.29	98.01	100.49
243.2	303.6	293.8	288.1	378.6	100.4	48.9	274.9	200.7	523.5	96.5
498.0	624.0	827.0	284.0	1080.0	256.0	180.0	181.0	575.0	392.0	310.0
306.9	1074.2	108.6	435.7	50.2	48.0	8.1	9.7	9.8	449.4	4.8
52.0	204.6	21.6	90.9	17.6	10.5	2.1	1.3	1.4	95.4	3.0
80.1	99.9	34.1	62.7	41.8	42.2	10.4	17.6	8.4	49.8	4.3
19176.4	0.0	42420.6	31047.6	61680.0	18014.2	8384.5	22829.1	22663.1	39515.1	10459.9
193.0	954.0	158.0	355.0	112.0	109.0	18.0	4.0	17.0	91.0	9.0
472.0	1806.0	325.0	647.0	231.0	211.0	35.0	7.0	32.0	193.0	15.0
22.9	58.4	20.5	42.6	14.1	10.5	15.2	3.8	6.0	16.9	7.5
97.6	112.3	77.3	136.0	97.0	36.9	453.8	6.2	6.3	36.5	9.9
1091.1	0.0	305.5	523.7	305.5	523.7	130.9	43.6	218.2	261.9	43.6
261.0	699.0	144.0	236.0	112.0	89.0	13.0	2.0	13.0	76.0	9.0
948.1	972.1	421.8	562.9	482.5	608.1	117.8	136.3	68.6	671.3	70.7
6294.7	0.0	2877.6	3237.3	3537.0	3597.0	899.2	1618.6	1618.6	4316.4	599.5
258.1	450.1	101.7	352.9	53.8	110.7	25.2	25.4	13.2	49.6	8.0
22.0	24.3	11.0	9.2	14.7	14.6	7.1	6.4	4.3	16.6	1.9
7.0	2.0	6.0	6.0	5.0	8.0	24.0	50.0	33.0	3.0	13.0
62.5	33.9	15.2	18.7	20.0	6.7	11.7	28.1	28.9	28.9	44.9
50.6	52.3	41.4	60.1	61.8	22.3	70.5	53.3	50.8	45.2	75.5
30.4	29.3	25.3	29.6	24.7	28.7	18.4	13.2	12.7	27.9	8.3
6.0	8.0	5.0	13.0	34.0	3.0	3.0	-4.0	1.0	4.0	10.0
82.0	60.0	40.0	54.0	16.0	16.0	12.0	50.0	7.0	76.0	487.0
10.0	7.0	9.0	4.0	8.0	4.0	2.0	8.0	3.0	9.0	8.0

* = samples that returned poor totals (<98.5%) after initial measurement were reweighed, ignited and fused. This made no difference to the totals, suggesting problems due to OH in micas or high levels of unmeasured elements (eg F, Cl).

APPENDIX B

	FHQ	YP		Mica schist	Amphibolite Gneisses		VALLEY FLOOR MAFICS			
HV-81	HV-55*	HV-77	HV-78	948-92-FHQ3	HV-46	HV-16	HV-17	HV-45*	HV-41	HV-74
Si 86.50	78.71	63.66	63.12	31.50	50.37	50.85	49.15	47.11	43.26	41.52
Al 6.35	4.95	20.52	19.83	24.91	13.41	12.09	15.30	14.71	15.00	15.44
Fe_2O_3 2.97	2.25	5.23	6.18	14.28	16.57	12.82	12.14	13.69	9.86	10.76
Mn 0.01	0.03	0.03	0.20	0.07	1.00	0.39	0.18	0.05	0.12	0.14
Mg 0.32	0.17	0.93	0.77	16.59	6.99	7.29	6.61	5.47	19.13	18.52
Ca 0.02	0.02	0.11	0.09	0.23	0.71	8.97	8.72	6.37	7.52	7.59
Na 0.11	0.11	0.21	0.24	0.35	0.06	0.74	2.59	5.96	1.31	1.17
K 2.50	2.17	5.39	5.11	7.73	1.96	1.27	1.91	1.19	0.58	0.35
Ti 0.28	0.16	0.55	0.59	0.72	2.32	3.13	1.91	1.55	0.20	0.16
P_2O_5 0.02	0.01	0.07	0.09	0.19	0.46	0.53	0.37	0.16	0.05	0.04
SO_3 -0.01	-0.01	0.00	0.00	0.00	0.00	0.00	0.03	0.10	0.03	0.03
LOI 0.90	0.57	3.43	3.21	2.77	5.35	0.72	0.45	0.93	3.89	4.85
99.98	89.16	100.13	99.43	99.34	99.19	98.81	99.35	97.29	100.94	100.57
Rb 103.8	101.3	351.3	299.6	1069.5	109.5	105.8	97.8	32.5	15.6	7.4
Ba 899.0	623.0	857.0	875.0	375.0	446.0	108.0	494.0	132.0	31.0	78.0
Th 9.9	6.2	34.3	36.9	29.5	82.3	2.7	2.0	4.9	0.5	-0.1
U 0.2	2.5	9.5	5.9	1.7	9.5	4.0	2.3	0.8	-1.8	-0.2
Nb 5.7	6.6	22.4	26.2	18.4	15.5	32.9	15.2	5.0	1.1	0.9
K 20753.7	18014.2	44745.0	42420.6	64170.5	16270.9	10542.9	15855.8	9878.8	4814.9	2905.5
La 15.0	13.0	69.0	59.0	75.0	11.0	32.0	37.0	16.0	0.0	0.0
Ce 34.0	29.0	133.0	130.0	141.0	59.0	85.0	80.0	46.0	6.0	8.0
Pb 4.7	6.6	20.1	33.5	8.4	71.2	9.0	7.1	3.0	0.3	2.4
Sr 19.5	19.4	35.3	26.4	5.7	27.5	119.1	138.2	257.7	147.4	110.3
P 87.3	43.6	305.5	392.8	829.2	2007.5	2313.0	1614.8	698.3	218.2	174.6
Nd 18.0	14.0	61.0	51.0	50.0	19.0	50.0	37.0	18.0	2.7	0.0
Zr 137.0	87.1	241.6	277.9	405.2	255.6	342.1	172.8	19.7	12.6	9.8
Sm							8.9		0.7	0.5
Ti 1678.6	959.2	3297.2	3537.0	4316.4	13908.4	18764.3	11450.4	9292.2	1199.0	959.2
V 11.9	11.2	57.0	55.5	93.2	48.9	91.4	54.3	31.7	3.8	2.6
Sc 1.9	2.3	14.8	14.7	10.1	50.2	57.2	28.0	33.1	7.3	5.6
Cr 19.0	18.0	51.0	53.0	39.0	77.0	109.0	222.0	49.0	149.0	1101.0
V 20.2	24.5	80.0	76.4	76.0	261.5	384.4	236.3	314.3	46.7	40.9
Co 92.0	60.6	18.5	21.8	59.2	55.3	40.1	59.4	37.7	113.9	105.0
Ga 10.9	11.3	30.0	32.2	38.6	25.7	25.4	24.3	26.0	13.0	16.5
Cu 7.0	4.0	21.0	33.0	-5.0	669.0	2.0	32.0	2.0	12.0	10.0
Zn 10.0	23.0	53.0	42.0	168.0	657.0	134.0	107.0	18.0	51.0	76.0
Ni 9.0	10.0	27.0	27.0	39.0	21.0	45.0	99.0	86.0	791.0	0.5

* = samples that returned poor totals (<98.5%) after initial measurement were reweighed, ignited and fused. This made no difference to the totals, suggesting problems due to OH in micas or high levels of unmeasured elements (eg F, Cl).

APPENDIX C:

ISOTOPE SYSTEMATICS

APPENDIX C: ISOTOPE SYSTEMATICS

Isotope geology relies on the radioactive decay of unstable atomic nucleii at a known rate. This rate is the half life of an isotope, or the period of time after which half of the mass of the radioactive isotope will have decayed to form a stable isotope. Half lives of radioactive elements range from incredibly short (thousandths of a second) to mindbogglingly large (the order of 10^{15} years, or older than the universe). For geological applications, the latter are preferred, but the isotopes must also be common enough to be accurately measured in order to be meaningful.

Radioactive decay may be generalised in the form of:

$$-(dN/dt) = lN \qquad \text{(eq 1)}$$

where N = the number of atoms remaining at time t,

and l = the decay constant for a given isotope system.

Therefore, the half life ($T_{1/2}$) is the time taken to reduce the number of parent atoms by half, and may be expressed as:

$$T_{1/2} = \ln 2/l \qquad \text{(eq 2)}$$

Also, $\ln N = -lt + \ln N_0$ (from eqn 1) which gives:

$$N_0 = Ne^{lt} \qquad \text{(eq 3)}$$

by rearrangement.

Assuming that the decay produces a stable daughter nuclide, it is possible to calculate the number of daughter nuclides:

$$D^* = N_o - N \qquad \text{(eq 4)}$$

because the number of daughter nuclides (D^*) produced equals the number of parent nuclides destroyed.

Substitution of (3) in (4) gives the geochronometry equation, which expresses the amount of daughter product at a given time in terms of N and l:

$$D^* = Ne^{lt} - N \qquad \text{(eq 5)}$$

A given sample may also originally have a certain number of atoms of the daughter nuclide in it that are not the result of radioactive decay (D_o), so the total number of daughter atoms (D) is the sum of the two:

$$D = D_o + D^* \qquad \text{(eq 6)}$$

Substitution and rearrangement of (5) and (6) give:

$$D = D_o + N(e^{lt} - 1) \qquad \text{(eq 7)}$$

In this form, both D and N may be measured, and l a constant which is determined experimentally. The age of a rock or mineral is obtained by solving for t, if some assumptions are made about D_o. In some cases, D_o is very small compared to D and may be ignored, but more commonly multiple samples from the same rock may be obtained (these samples therefore have the same age, t, and the same initial amount of the daughter, D_o) in which case (7) is a straight line when plotted against D and N. The age of the samples is therefore the slope (m) of (7), ie:

$$m = e^{lt} - 1 \qquad \text{(eq 8)}$$

and $$t = 1/l(\ln(m+1)) \qquad \text{(eq 9)}$$

where t is the age of the rock.

However, in practice it is easier to measure the ratios of isotopes on a mass spectrometer than the absolute values of D and N. Therefore, for a given isotopic system, all isotopes are measured relative to a stable isotope, and D and N are expressed as ratios. Therefore, D_o of (7) is the y intercept of the isochron, and is known as the initial ratio for the system.

In practical terms, (9) becomes:

$$t = 1/l(((D^*/S) - (D_o/S))/(N/S) + 1) \qquad \text{(eq10)}$$

where S is the number of atoms of the stable isotope.

For the Rb-Sr isotope system, S is ^{86}Sr, and in Sm-Nd S is ^{144}Nd.

For each of these systems it is also possible to calculate a model age for the sample. The model age is an age calculated relative to the presumed source of the material, ie the mantle, and therefore reflects the presumed age of extraction from this source. Two kinds of mantle are considered, a uniformly evolving mantle (CHUR) and a depleted mantle that has experienced a single major depletion event.

Model age is therefore:

$$T_{mod}CHUR = 1/l(m/((N/S) - (N/S)_{CHUR}) + 1) \quad \text{(eq 11)}$$

For a model age relative to the depleted mantle, N/S_{dep} is substituted for CHUR. Model ages for the Rb-Sr system are rarely significant due to the mobility of the parent and daughter nuclides, however in the Nd-Sm system model ages may be preserved into the sedimentary cycle, thus reflecting the age from which that material was derived from the mantle.

A more convenient way of expressing Nd values is the epsilon (ε) notation, which is the parts per 10000 difference between the sample and CHUR. ε notation can also be calculated for Rb-Sr, but is not as meaningful due to the resetting referred to above, and is rarely used.

$$\varepsilon^t_{Nd} = (((^{143}Nd/^{144}Nd)^t_{sample} / (^{143}Nd/^{144}Nd)^t_{CHUR}) - 1) * 10000 \quad \text{(eq 12)}$$

Therefore, for a given time, t, it is possible to calculate ε values, and then extrapolate the evolution of that sample (usually an igneous rock) back in time to its time of departure from the mantle (or model age). Comparison of ε values and model ages are powerful tools in understanding the timing of crustal additions from the mantle and evolution of a terrain over time.

The isotopes and constants used in the decay schemes described in this study are summarised below:

		Rb-Sr	**Sm-Nd**
	l:	$1.42 \pm 0.01 \times 10^{-11}$	$6.54 \pm .05 \times 10^{-12}$
CHUR:		$^{87}Rb/^{86}Sr = 0.0827$	$^{147}Sm/^{144}Nd = 0.1966$
		$^{87}Sr/^{86}Sr = 0.70450$	$^{143}Nd/^{144}Nd = 0.512638$
Depleted Mantle:		$^{87}Sr/^{86}Sr = 0.7027 \pm 5$	$^{143}Nd/^{144}Nd = 0.5132 \pm 1$

APPENDIX D:

SUMMARY OF ISOTOPIC DATA

All samples are prefixed A1015-; except those
prefixed 948-92- and 92-2-

APPENDIX D: Isotope data.

	BRITISH EMPIRE GRANITE					PARAGNEISSES			FHQ	YP	
sample no.	948-92-BE1	948-92-BE2	948-92-BE3	948-92-BE4	HV-56	948-92-FHQ1	948-92-FHQ2	948-92-FHQ3	HV-55	HV-78	HV-65
Nd ppm	10.217	6.441	7.535	5.649	2.246	19.686		20.146	16.881	53.357	80.076
Sm ppm	2.403	1.664	1.880	1.370	0.815	3.467		3.677	2.995	9.977	15.432
143/144 Nd	0.511826	0.511787	0.511865	0.511781	0.512039	0.511420	0.514283	0.511536	0.511493	0.511539	0.511699
2 sigma	0.0000590	0.0000590	0.0000590	0.0000590	0.0002469	0.0000590	0.0000590	0.0000460	0.0000530	0.0003360	0.0001720
Sm/Nd	0.2352	0.2583	0.2496	0.2425	0.3626	0.1761		0.1825	0.1774	0.1870	0.1927
147Sm/144Nd	0.1423	0.1563	0.1510	0.1467	0.2193	0.1065		0.1104	0.1073	0.1131	0.1166
143/144Nd ch	0.512638	0.512638	0.512638	0.512638	0.512638	0.512638	0.512638	0.512638	0.512638	0.512638	0.512638
143/144Nd dep	0.513108	0.513108	0.513108	0.513108	0.513108	0.513108	0.513108	0.513108	0.513108	0.513108	0.513108
T mod:chur	2.26	3.19	2.56	2.60		2.05		1.94	1.95	2.00	1.78
T mod:dep	2.65	3.36	2.91	2.91		2.35		2.27	2.26	2.32	2.16
eps Nd (0)	-15.83963733	-16.60040809	-15.07886657	-16.71744974	-11.68758461	-23.75945599		-21.49665066	-22.33544919	-21.43812983	-18.31701903
Sr87/86	0.979981	0.921056	0.901534	0.864247	0.941522	2.317549	2.311550	4.429876	0.967251	1.186214	0.899046
2 sigma	0.000049	0.000049	0.000049	0.000049	0.000049	0.000049	0.000049	0.000049	0.000084	0.000330	0.000228
Sr ppm	35.36	38.603	47.744	61.706	26.02928	5.366	6.067	6.93439	19.60018	26.42413	95.56716
Rb ppm	489.545	290.114	320.898	245.989	231.4518	272.984	199.945	1056.15	102.3064	287.6497	360.609
Rb/Sr	13.8446	7.5153	6.7212	3.9865	8.8920	50.8729	32.9562	152.3061	5.2197	10.8859	3.7734
87Rb/86Sr	6536.775571	2295.703044	2808.745287	1650.477887	1461.165675	2032.603749	1090.434121	30424.92685	285.4854254	2256.868146	3546.920539
Sr T Mod Dep	0.472944583	0.689262755	0.703064505	0.965792277	0.636056116	0.664341812	1.019795483	0.435276491	1.194359956	1.025690807	1.234570229
Sr T Mod Chn	0.47111702	0.686211764	0.699669433	0.960814728	0.633413495	0.663940485	1.019287337	0.435149514	1.191115152	1.023993881	1.230168522

all wrong!
TOOLKIT!

* Samples 948-92-BE1 to BE4 and 948-92-FHQ1-3 from Foden (*unpubl. data*).
Samples with <1ppm Sm produced unacceptable within run statistics, and hence data for such samples is incomplete.

APPENDIX D: Isotope data.

ORTHOGNEISSES					VALLEY FLOOR MAFICS			MT NEILL GRANITE			
HV-80	**HV-84**	**HV-86**	**HV-66**	**HV-60**	**HV-17**	**HV-41**	**HV-74**	**HV-12**	**HV-13**	**HV-48**	**HV-57**
108.410	18.65884	132.7122	111.9166	3.796645	34.15411	2.656501	2.48135	14.85199	12.39371	34.15411	136.8616
19.830	3.645642	27.77311	21.58282	0.7727457	6.979845	0.7315924	0.5089223	3.85877	3.383583	6.979845	32.92772
0.511718	0.511894	0.51157	0.511773997		0.512022562			0.511827261	0.51186461	0.51171566	0.5117222
0.0000930	0.0001060	0.0000388	0.0000225		0.0000338			0.0000422	0.0000852	0.0000693	0.0001228
0.1829	0.1954	0.2093	0.1928	0.2035	0.2044	0.2754	0.2051	0.2598	0.2730	0.2044	0.2406
0.1106	0.1182	0.1266	0.1167	0.1231	0.1236	0.1666	0.1241	0.1572	0.1651	0.1236	0.1455
0.512638	0.512638	0.512638	0.512638	0.512638	0.512638	0.512638	0.512638	0.512638	0.512638	0.512638	0.512638
0.513108	0.513108	0.513108	0.513108	0.513108	0.513108	0.513108	0.513108	0.513108	0.513108	0.513108	0.513108
1.63	**1.44**	**2.31**	**1.64**		**1.28**			**3.10**	**3.70**	**1.92**	**2.71**
2.01	**1.89**	**2.62**	**2.05**		**1.79**			**3.31**	**3.71**	**2.29**	**2.99**
-17.94638712	**-14.51316524**	**-20.83341461**	**-16.85405686**		**-12.00531759**			**-15.81503127**	**-15.08647428**	**-17.99203336**	**-17.86445796**
1.070056	0.736853	0.922266	0.938147	0.724007	0.743872	0.707388	0.706934	0.823401	1.210918	0.792262	1.027965
0.000356	0.000323	0.000172	0.000048	0.000049	0.000049	0.000049	0.000049	0.000049	0.000049	0.000049	0.000049
74.96491	316.7385	121.6859	91.90439	539.5245	134.9303	147.5659	109.9608	38.57176	33.44392	56.42044	46.94116
276.1867	184.2011	252.333	216.9862	77.06058	93.79074	14.94603	7.99914	106.2098	826.7278	87.44424	397.7547
3.6842	0.5816	2.0736	2.3610	0.1428	0.6951	0.1013	0.0727	2.7536	24.7198	1.5499	8.4735
2080.57731	1.68738727	1736.706534	6.984968285	161.9730958	239.9375726	6.092983967	1.745279276	307.6858457	18642.46856	208.5646741	4315.279958
2.312503418	1.430808621	2.493647473	2.345561041	3.892760659	1.438803838	1.192507638	1.59838129	1.049048292	0.475163378	1.388267188	0.900486265
2.311435588	1.40475137	2.492728559	2.344029007	4.017171537	1.417340794	0.955413567	1.317834202	1.042151615	0.474163808	1.378513896	0.898099808

* Samples 948-92-BE1 to BE4 and 948-92-FHQ1-3 from Foden (*unpubl. data*).
Samples with <1ppm Sm produced unacceptable within run statistics, and hence data for such samples is incomplete.

APPENDIX E:

ANALYTICAL PROCEDURES

APPENDIX E: Analytical Procedures

Isotope Analysis:

Samples were selected on the basis of freshness and size before being cut by diamond saw to remove weathered surfaces. They were then crushed in a jaw crusher and milled in a tungsten carbide mill.

Sample dissolution was carried out in teflon vials using HF and HF-HNO_3. Samples were then converted to a chloride and split, with half the sample being spiked with ^{150}Nd-^{147}Sm spike solution.

The Rb-Sr fraction was separated using cation exchange columns, with the residue being collected and used on a second set of columns (teflon + EDEHP) to extract Sm and Nd fractions.

Sr samples were mounted onto single tantalum filaments, whereas Sm and Nd samples were mounted onto double tantalum-rhenium filaments. Analysis was carried out on a Finnigan MAT 261 solid source mass spectrometer, with measurements collected in data blocks of 11 scans each. Measurement was continued until statistics during the run were within standard operating conditions.

XRF Analysis:

Samples were milled in the manner described above, then used to produce fused discs for whole rock analysis and pressed pellets for trace elements. Pressed pellets were made by mixing the sample powder with binding solution and compressing to produce a smooth, flat face. Fused discs were produced by igniting ~2 grams of powder at 960°C overnight to determine the percentage loss of volatiles. Ignited samples were then mixed with ~4 grams of flux for each gram of sample, and then fused on the Norrish Prometheus Fusion Apparatus.

Analysis of both pressed pellets and fused discs was carried out by X-ray Fluorescence (XRF) on a programmable Phillips PW 1480 X-ray spectrometer.

APPENDIX F:

GEOLOGICAL MAP AND BLOCK DIAGRAMS OF THE PARALANA HOT SPRINGS - HIDDEN VALLEY AREA